8-2018

Rotary pump speed modulation to produce pulsatile flow and ventricular volume unloading.

Connor Joseph Smith
University of Louisville

ROTARY PUMP SPEED MODULATION TO PRODUCE PULSATILE FLOW AND
VENTRICULAR VOLUME UNLOADING

By

Connor Joseph Smith
B.S., University of Louisville, 2017

A Thesis
Submitted to the Faculty of the
University of Louisville
J. B. Speed School of Engineering
as Partial Fulfillment of the Requirements
for the Professional Degree

MASTER OF ENGINEERING

Department of Bioengineering

July 2018

ROTARY PUMP SPEED MODULATION TO PRODUCE PULSATILE FLOW AND
VENTRICULAR VOLUME UNLOADING

Submitted by:‗‗‗‗‗‗‗‗‗‗‗‗‗‗‗‗‗‗‗‗‗‗‗‗‗‗‗

Connor Joseph Smith

A Thesis Approved On

‗‗‗‗‗‗‗‗‗‗‗‗‗‗‗‗‗‗‗‗‗‗‗‗‗‗‗

(Date)

by the Following Reading and Examination Committee:

‗‗‗‗‗‗‗‗‗‗‗‗‗‗‗‗‗‗‗‗‗‗‗‗‗‗‗

Steven C. Koenig, Ph.D., Thesis Director

‗‗‗‗‗‗‗‗‗‗‗‗‗‗‗‗‗‗‗‗‗‗‗‗‗‗‗

Kevin G. Soucy, Ph.D.

‗‗‗‗‗‗‗‗‗‗‗‗‗‗‗‗‗‗‗‗‗‗‗‗‗‗‗

Elizabeth A. Gentry, Ph.D.

‗‗‗‗‗‗‗‗‗‗‗‗‗‗‗‗‗‗‗‗‗‗‗‗‗‗‗

Gretel Monreal, Ph.D.

ACKNOWLEDGEMENTS

Finally, thank you to my mother and father for their constant support and encouragement throughout my academic career. I would not have accomplished anything without your help. A special thanks to my fiancée for her unwavering support and encouragement during this time.

ABSTRACT

Background: Continuous-flow (CF) left ventricular assist devices (LVADs) have gained widespread clinical acceptance as a treatment option for advanced heart failure (HF); however, they have also been associated with an increased risk of adverse events, including gastrointestinal bleeding, aortic insufficiency, and hemorrhagic stroke. It has been hypothesized that the increase in adverse event incidence may be due in part to diminished vascular pulsatility and high shear stress when CF-LVADs are operated at fixed speeds. Previous studies have shown that pump speed modulation generates greater levels of pulsatility in rotary pumps than when operated at fixed speeds. The objective of this study was to characterize the hemodynamic and pump performance of LVADs operated with a low-frequency asynchronous pump speed modulation algorithm in a chronic healthy bovine model with partial VAD support.

Materials and Methods: Clinical-grade LVAD with aortic (HeartWare HVAD, n=3) or transaortic (proprietary VADx, n=4) outflow were implanted into chronic (30-day) healthy male Jersey calves (60-110 kg). An asynchronous pump speed modulation algorithm (frequency = 20 bpm, amplitude = 2500-4000 RPM for HVAD or 11000-19000 RPM for VADx) was implemented by controlling pump current. Hemodynamic measurements (pressures, flows) were recorded throughout the study duration (30s epochs collected

hourly at 400Hz), echocardiographic data was recorded during the implant, weekly, and at terminal, and blood laboratory measurements were regularly collected throughout the study. All data were analyzed to characterize aortic pulsatility, LV unloading, blood damage, and device power usage. Statistical analysis was performed to determine significance between fixed and pump speed modulation operating conditions.

Results and Discussion: Two HVAD and four VADx animals achieved the 30-day study endpoint. Due to surgical complications, one animal died intraoperatively. Both HVAD devices maintained asynchronous modulation for the full study duration with mean high and low speeds of 4000 RPM and 2500 RPM, respectively. Two of the four VADx devices maintained asynchronous modulation at average high and low speeds of 17238 RPM and 11333 RPM over the 30-day study; however, the other two VADx devices operated at fixed pump speed for 1 and 2 days, respectively, due to unforeseen controller malfunctions, which were corrected to restore asynchronous modulation. Near-physiologic aortic pulse pressure for HVAD (45±4 mmHg) and VADx (46±9 mmHg) was demonstrated. HVAD and VADx with asynchronous modulation reduced stroke volume by 27% and 23%, respectively. HVAD (n=2) and VADx (n=3) maintained plasma free hemoglobin (pfHb) less than 40 mg/dL for the entire study duration while one VADx had pfHb > 40 mg/dL for a period of 3 days, which resolved. Asynchronous modulation increased power consumption with HVAD (25%) and VADx (6%) compared to fixed speed operation.

Conclusion: This study demonstrated asynchronous modulation of HVAD and VADx maintained near-physiologic pulsatility and LV unloading at the expense of minimal hemolysis and increased power consumption in the partial VAD support model. Future studies in clinically-relevant heart failure models warrant further investigation.

TABLE OF CONTENTS

LIST OF TABLES

LIST OF FIGURES

I. BACKGROUND

A. <u>Cardiovascular Physiology: A Healthy Heart</u>

A normal human heart is comprised of 4 chambers which allows the complete separation of the deoxygenated and oxygenated blood increasing the efficiency of nutrient exchange in the circulation. Deoxygenated blood returns from the systemic circulation through the superior and inferior vena cava and enters the right atrium (RA) and then the right ventricle (RV) through the tricuspid valve. It then leaves the RV through the pulmonary valve and pulmonary artery and travels through the pulmonary circulation where it become oxygenated and returns to the heart via the pulmonary veins. The pulmonary veins empty into the left atrium (LA), and the oxygenated blood enters the left ventricle (LV) through the mitral valve. Blood is ejected from the LV and crosses the aortic valve and flows through the aorta and the systemic circulation. An illustration summarizing the complete systemic and pulmonary circulations is shown in Figure 1.
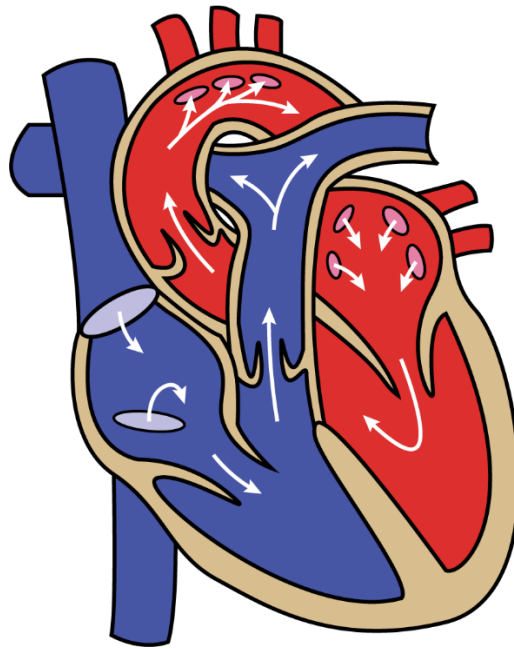
FIGURE 1: The path of blood flow through the heart. Blood flow begins with the pulmonary circulation (blue) to oxygenate blood which is returned to the LA and pumped into the systemic circulation (red). Blood flow direction is depicted by white arrows.

A cardiac cycle consists of periods of low pressure (diastole) and high pressure (systole). During diastole the heart muscle relaxes from its contracted systolic state, blood flows from the atria into the ventricles, and pressure builds in the heart due to the increasing volume (preload). The end of diastole occurs when the atria contract and empty the remaining blood volume into the ventricles. Systole occurs directly after when the ventricles begin to isometrically contract increasing ventricular pressure until it is greater than the pressure in the corresponding circulations (afterload). At this point, the pulmonary and aortic valves are forced open and blood is ejected from the ventricles into the circulations. Relaxation and diastole immediately follow, and the cardiac cycle resumes.

Typical hemodynamic waveforms for a healthy heart can be seen in Figure 2. Aortic pressure (AoP) reaches about 120 mmHg during systole and falls to around 80 mmHg during diastole. Left ventricular pressure (LVP) is around 5 mmHg during diastole and

increases slightly as the ventricle fills with blood. During isovolumic contraction, LVP increases to the diastolic AoP and then blood is ejected with LVP reaching about 120 mmHg. Left ventricular volume (LVV) usually increases from 50 mL at the end of systole to about 120 mL at the end of diastole. Therefore, the amount of blood ejected from the heart in one cardiac cycle (stroke volume; SV) is about 70 mL which makes the amount of blood pumped by the heart per minute (cardiac output; CO) typically about 4-8 L/min (Kemp & Conte, 2012).
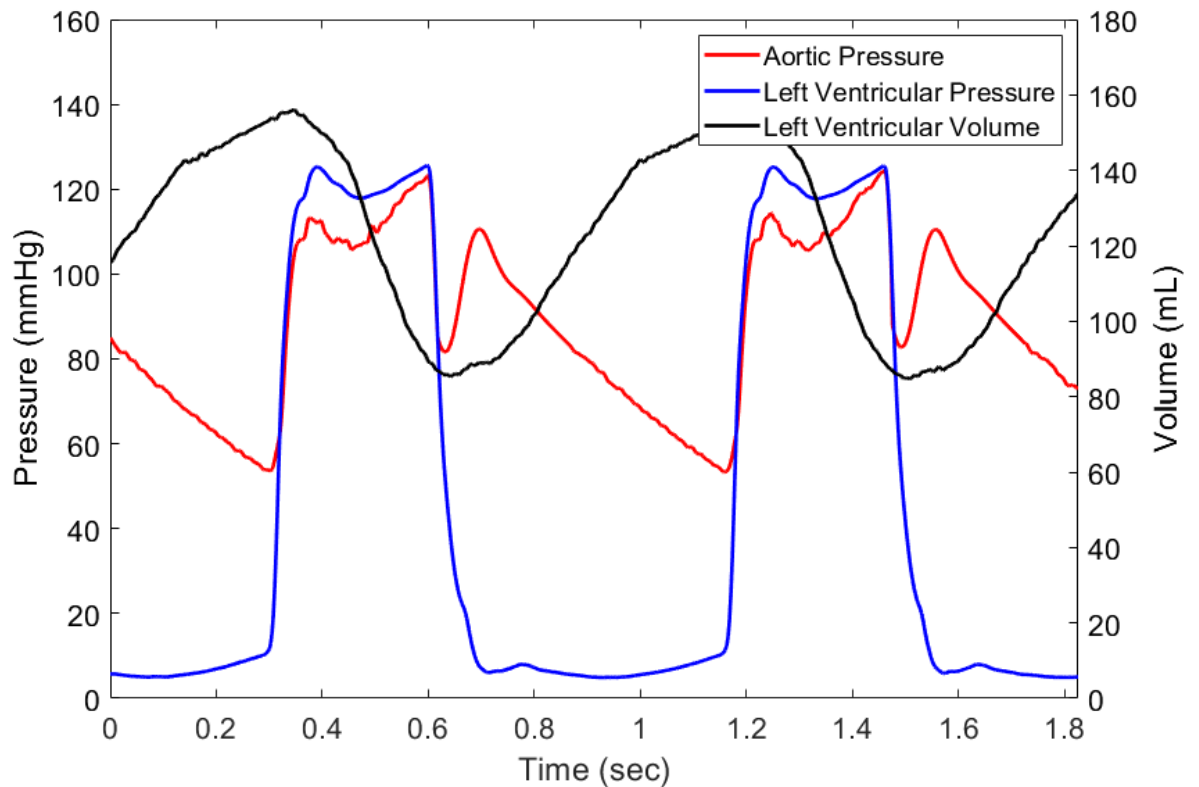
FIGURE 2: Hemodynamic waveforms recorded in a mock circulatory loop tuned to healthy heart conditions. In a healthy heart, aortic pressure is around 120 mmHg during systole and 80 mmHg during diastole. LVP is about 5 mmHg during diastole and reaches about 120 mmHg during contraction and systole. A typical normal SV and CO is about 70 mL and 4-8 L/min, respectively.

Regulation of the heart contraction is controlled by the rate of venous return and the effects of the autonomic nervous system on the myocardium. Sympathetic stimulation serves to increase the force of contraction of the heart muscle to as much as double the normal effort which increases the SV and the blood's ejection pressure from the ventricle, effectively increasing CO (Hall & Guyton, 2011). Inhibition of the sympathetic stimulation results in reduction of cardiac output by decreasing the strength of ventricular contraction and the heart rate (HR). Parasympathetic stimulation via the vagus nerve mainly serves to decrease the HR while also reducing the strength of the myocardial contraction, effectively decreasing CO (Hall & Guyton, 2011).

While the autonomic nervous system can control the contractile force and the rate of contraction of the heart muscle to affect CO, the main determinant of CO is the rate of venous return of blood into the atria and ventricles (Hall & Guyton, 2011). The heart possesses an intrinsic ability to respond to increasing volumes of venous return. It efficiently pumps all blood that returns to it from the veins within physiological limits, and this phenomenon is known as the Frank-Starling mechanism. A graphical representation of this phenomenon can be seen in Figure 3. With increasing venous return, the end-diastolic volume (LVEDV) of the LV increases and stretches the myocardium increasing end-diastolic pressure (LVEDP) and the tension between the underlying actin and myosin filaments which provides for a greater force during muscle contraction. The increase in the contractile force causes a nonlinear increase in SV and CO.
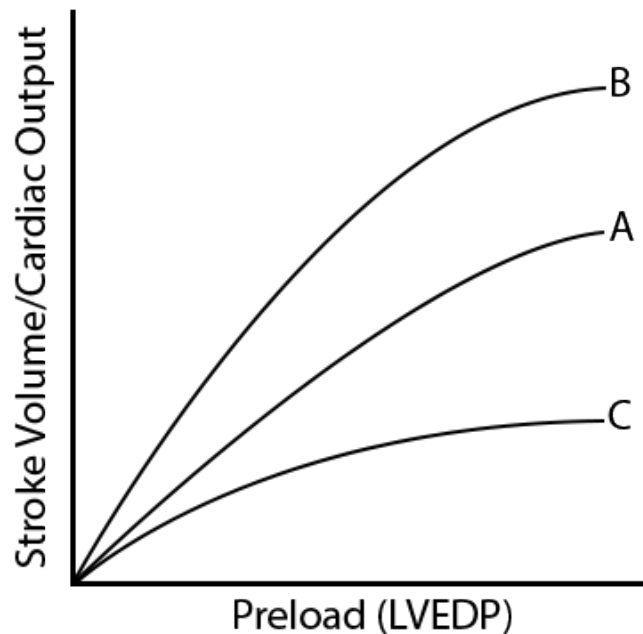
FIGURE 3: The Frank-Starling mechanism as represented by three conditions: A) normal healthy heart, B) increased myocardial contractility, C) dysfunction of the heart such as in heart failure (HF). As preload increases, cardiac output increases nonlinearly until the heart can no longer compensate for the additional blood volume. When the heart experiences increased contractility, cardiac output increases more for the same increase in preload compared to normal function. During heart failure, the heart is unable to efficiently eject blood and can no longer adequately compensate for increases in preload.

Mean arterial pressure (MAP) is the afterload which the heart must contract against to eject blood and is a product of the CO and the total peripheral resistance (TPR) of the vasculature. An increase in afterload lowers the efficiency of ventricular contractility and shifts the Frank-Starling curve down and to the right. The renin-angiotensin-aldosterone system (RAAS) is important in regulating vascular resistance and blood volume by its downstream effects of vasoconstriction and salt and fluid retention (Klabunde, 2012). When patients develop HF, the overstimulation of the Frank-Starling mechanism and the

RAAS can cause a decrease in CO and SV leading to a cycle which results in a decreased MAP and worsening of HF symptoms.

<p style="text-align:center">B. <u>Heart Failure Physiology</u></p>

1. <u>Symptoms and Classification</u>

Over 22 million people are currently estimated to be living with heart failure worldwide, and the U.S. prevalence is expected to rise to 3% or over 8 million people by 2030 (Heidenreich et al., 2013). Heart failure can be defined as the heart's inability to meet the metabolic needs and oxygenation requirements of the body due to an inadequate maintenance of CO (Kemp & Conte, 2012; Tanai & Frantz, 2015). Due to the heart's inability to properly eject all blood which enters the ventricles, blood volume can build in the pulmonary capillary bed during heart failure increasing pressure and leading to symptoms of pulmonary congestion such as dyspnea, cough, and wheezing (Kemp & Conte, 2012; Tanai & Frantz, 2015). Renal dysfunction can result from venous congestion and/or hypoperfusion during heart failure and can lead to malabsorption and cardiac cachexia with the loss of body tissue (Pearse & Cowie, 2014; Tanai & Frantz, 2015). Fatigue, palpitations, and nausea can also occur due patients' low CO, and patients can develop anemia which can be worsened by their renal dysfunction (Kemp & Conte, 2012; Pearse & Cowie, 2014; Tanai & Frantz, 2015).

Heart failure is a progressive disease that can be characterized by the affected ventricle (left- or right-sided) or the impaired portion of the cardiac cycle (systolic or diastolic). Left-sided heart failure is caused by left ventricular dysfunction, and right-sided heart failure is a weakening of the right ventricle which often occurs due to fluid backup in the lungs caused by left-sided heart failure. Systolic heart failure results from impaired left

ventricular contractility and is referred to as heart failure with reduced ejection fraction (HF-REF) that is diagnosed with an EF less than 40% (Pearse & Cowie, 2014; Tanai & Frantz, 2015). If patients present with heart failure symptoms but have an EF between 40-50%, this is referred to as heart failure with preserved ejection fraction (Pearse & Cowie, 2014; Tanai & Frantz, 2015). Chronic heart failure patients develop worsening symptoms over time, while acute heart failure is characterized by a more rapid onset of cardiac dysfunction and clinical symptoms such as congestion, renal dysfunction, and low cardiac output (Krum & Abraham, 2009; Metra & Teerlink, 2017).

The New York Heart Association (NYHA) has classified the progression of heart failure based on the patient's clinical condition (Apostolakis & Akinosoglou, 2007; Kemp & Conte, 2012). Class I HF represents patients who present no symptoms. Class II HF patients are comfortable at rest while having slight limitation in physical activity due to HF symptoms, and Class III patients present HF symptoms with mild physical activity while being comfortable at rest. Finally, Class IV patients are unable to perform any physical activity without HF symptoms emerging. Similarly, the American Heart Association (AHA) has classified the disease's progression, however their distinctions dwell on the structural abnormality of the heart (Kemp & Conte, 2012). Patients who are at high risk for HF but do not present any symptoms or structural disorders are said to be in Stage A HF. Those that present with structural abnormalities but no HF symptoms are in Stage B HF, and Stage C HF patients display symptoms of HF and have structural abnormalities. Finally, patients in Stage D are said to be in end-stage conditions and require specialized interventions and treatment strategies. AHA and NYHA classifications can both be utilized and have some overlap in that Stage B corresponds to Class I, Stage C corresponds to Class

II and II, and Stage D corresponds to Class IV, while Stage A has no corresponding NYHA classification (Kemp & Conte, 2012; Mazurek & Jessup, 2015).

TABLE I

CLASSIFICATIONS OF HEART FAILURE AND THEIR DESCRIPTIONS

AHA Stages of HF	Equivalent NYHA Functional Classification
A – At high risk for HF but has no symptoms or structural disorders	None
B – No symptoms of HF but has some structural cardiac abnormalities	Class I – No limitation of physical activity and ordinary activity does not cause breathlessness or fatigue.
C – Displays symptoms of HF and has structural abnormalities	Class I – No limitation of physical activity and ordinary activity does not cause breathlessness or fatigue. Class II – Slight limitation of physical activity. No symptoms while at rest. Ordinary physical activity results in symptoms of HF. Class III – Marked limitation of physical activity. No symptoms while at rest. Less than ordinary activity results in HF symptoms. Class IV – Unable to carry on any physical activity without discomfort. Can have HF symptoms at rest.
D – Refractory HF requiring specialized interventions and treatment strategies	Class IV – Unable to carry on any physical activity without discomfort. Can have HF symptoms at rest.

2. Etiology

Since HF can be classified in many different ways, the underlying causes of the disease can vary greatly in patients. HF often advances from intrinsic abnormalities in myocardial structure and function which have been termed cardiomyopathies (Mazurek & Jessup, 2015). The most common cause of cardiomyopathies and HF is coronary artery disease (CAD) (Mazurek & Jessup, 2015; Pearse & Cowie, 2014). Ischemic

cardiomyopathies (ICM) resulting from a restriction of blood supply to the cardiac tissue such as from CAD, myocardial infarction, and toxins such as alcohol are more common in the developed world (Pearse & Cowie, 2014; Tanai & Frantz, 2015). Hypertension and valvular diseases such as stenosis or insufficiency are also common, however their significance has decreased with improved clinical management (Pearse & Cowie, 2014). Nonischemic cardiomyopathies (NICM) such as dilated cardiomyopathy (DCM) or hypertrophic cardiomyopathy (HCM) are less common and may be the result of genetic inheritance (Mazurek & Jessup, 2015). Other clinical conditions that are independent risk factors for HF are diabetes, obesity, smoking, cardiac arrhythmias, and congenital heart defects (Tanai & Frantz, 2015).

3. Pathophysiology

The development of heart failure is generally regarded to begin with an index event such as an abrupt myocardial infarction or prolonged myocardial ischemia that leads to activation of compensatory mechanisms that work to maintain MAP, CO, and adequate peripheral perfusion (Mazurek & Jessup, 2015; Pearse & Cowie, 2014). Compensatory mechanisms that are activated by the index event include ventricular remodeling, activation of the RAAS, and the Frank-Starling mechanism (Kemp & Conte, 2012). The prolonged activation of these mechanisms eventually begins to have detrimental effects on cardiac function and leads to the development of HF.

The Frank-Starling mechanism has a greater role in the initial compensatory response to a reduced CO. Increasing amounts of preload result in smaller increases in CO as the contractile limits of the heart are reached. In HF, a given increase in preload results in a smaller increase in CO compared to a healthy heart due to the diminished contractility. As

a patient's HF symptoms worsen with increased preload, the response in CO decreases further, and this compensatory mechanism eventually reaches its limits resulting in pulmonary congestion and reduced CO (Kemp & Conte, 2012). The result of this effect can be seen in Figure 4 as the pressure-volume (PV) loop shifts to the right as preload increases. LV end-diastolic pressure (EDP) increases, and end-systolic pressure (EDP) decreases which reduces stroke work (SW; area under curve).
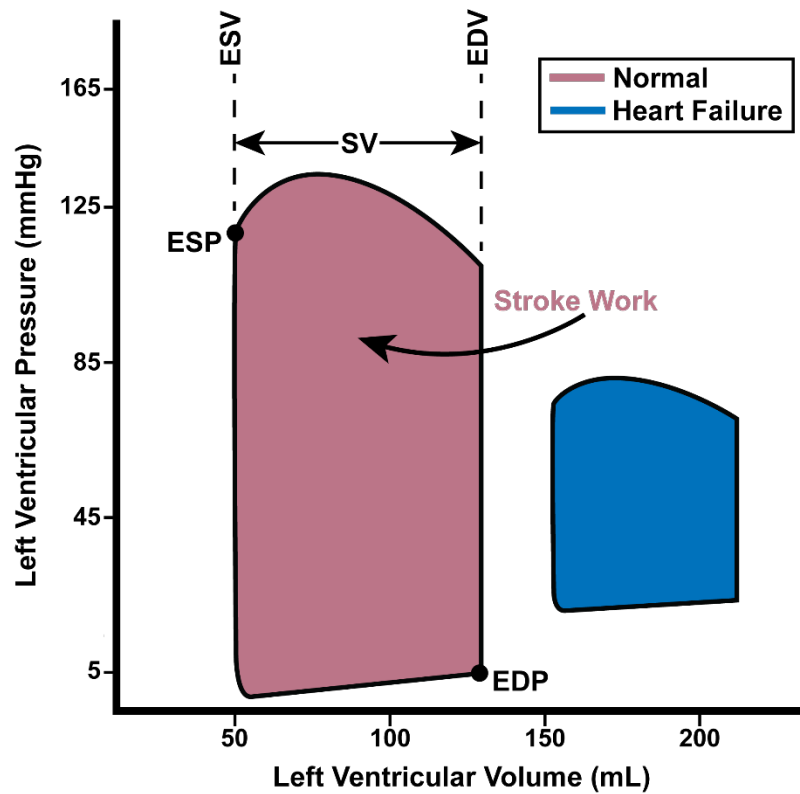
FIGURE 4: Effects on PV relationship due to HF. During heart failure, preload increases as the heart can no longer efficiently eject blood. This leads to rightward shift (red to blue) of the PV loop which also reduces in size due to decreased contractility. ESV: end-systolic volume; EDV: end-diastolic volume; ESP: end-systolic pressure; EDP: end-diastolic pressure; SV: stroke volume.

Ultimately, stimulation of these mechanisms for lengthy periods of time cause a positive feedback loop to develop. The diminishing returns of the Frank-Starling mechanism with very high levels of preload result in severely reduced CO leading to

extended activation of the RAAS eventually resulting in myocardial fibrosis and ventricular remodeling such as dilation and thinning of the ventricular wall and septum. The ventricular remodeling results in a worsening myocardial function and performance in turn decreasing the effectiveness of the Frank-Starling mechanism further. Thus, the disease progresses, and patients' clinical conditions worsen.

C. Heart Failure Therapy

1. Pharmacological Management

NYHA Class II patients are primarily treated by the use of oral cardiovascular medication such as β-blockers and drugs which block the effects of aldosterone (Gilbert & Xu, 2017). ACE Inhibitors (ACEIs) were one of the first pharmacological treatments which improved mortality and symptoms in HF-REF patients (Krum & Teerlink, 2011; Mazurek & Jessup, 2015). ACEIs block the conversion of angiotensin I to angiotensin II and prevent the downstream release of aldosterone thereby promoting blood vessels to dilate and reducing blood pressure. Angiotensin receptor blockers (ARB) prevent aldosterone release by directly blocking angiotensin II from binding to its receptor. ARBs are used less often than ACEIs and are mainly indicated for use when ACEIs are not well tolerated (Yancy et al., 2013). Aldosterone antagonists or mineralocorticoid receptor antagonists (MRA) may be used if ACEIs/ARBs administration is shown to be ineffective. MRAs block the effect of aldosterone at its receptor and were found to reduce the risk of death and hospitalization in patients treated with standard HF therapy of ACEIs/ARBs and β-blockers (Zannad et al., 2011). β-blockers prevent the binding of norepinephrine and epinephrine to the major classes of β adrenergic receptors (β-ARs: β_1, β_2) and therefore decrease contractility and heart rate which helps to manage high blood pressure, angina, and arrhythmias. In a meta-

analysis of all randomized, controlled clinical trials investigating β-blockers, Al-Gobari et al found that β-blockers reduce the risk of death by 33% and the risk of sudden cardiac death (SCD) by 31% (Al-Gobari et al., 2013). For patients experiencing congestion and volume overload, diuretics may be used to reduce preload and relieve symptoms (Krum & Abraham, 2009).

2. Implantable Cardioverter Defibrillators and Cardiac Resynchronization Therapy

Additional interventions may be needed for patients who are deemed to be in Stage C heart failure (NYHA Class II, III, IV) and diagnosed with HF-REF. These patients have an increased risk for SCD and ventricular arrhythmias and may undergo placement of an implantable cardioverter defibrillator (ICD) for arrhythmia monitoring and correction (Mazurek & Jessup, 2015). In addition, patients who have experienced incidents of ventricular fibrillation or ventricular tachycardia may undergo ICD implant for secondary prevention of SCD (McMurray, 2010). ICDs are implanted within the chest and are connected to the heart via electrical leads. The devices work to detect abnormal heart rhythms and send an electrical shock to the heart to restore a normal heartbeat. A meta-analysis of 14 different randomized, controlled trials and longitudinal, nonrandomized, comparative studies investigating the benefit of ICDs showed a decrease in the incidence of SCD and all-cause mortality due to ICD use (Earley et al., 2014).

Biventricular pacemakers are similar to ICDs and are also connected to the heart via electrical leads. These devices are used to provide cardiac resynchronization therapy (CRT) to treat ventricular dyssynchrony by monitoring and controlling the HR with electrical stimulation. They have been shown to immediately improve cardiac performance, reduce mitral regurgitation caused by the dyssynchrony, and increase the SV (Dickstein et al.,

2008; Hunt et al., 2009). This therapy has been shown to be more beneficial in NYHA Class I and II patients with widened QRS intervals than in Class III patients with narrowed QRS intervals (McMurray, 2010).

3. <u>Mechanical Circulatory Support</u>

NYHA Class III and IV patients whose HF symptoms continue to worsen despite medical therapy may require advanced clinical interventions. Mechanical circulatory support (MCS) has become increasingly used to treat and manage these patients due to the limited number of donor hearts available for HT. MCS devices may be used to restore myocardial performance (bridge-to-recovery; BTR), support patients until a donor heart can be procured (bridge-to-transplant; BTT), or for primary relief of HF symptoms without the goal of heart transplant (HT) or device removal (destination therapy; DT). The number of adult HT recipients who were previously treated with MCS devices has increased in the past decade and is about 40% (Andrew & Macdonald, 2015; Hullin, 2014).

4. <u>Heart Transplant</u>

Dr. Christiaan Barnard performed the first human to human heart transplant in South Africa in 1967. However, the procedure was not widely adopted until the 1980s when immunosuppression drugs were introduced that improved transplant outcomes. In a HT procedure, a donor heart is secured from an organ donor who has been determined to have similar biological profile to the recipient. The failing heart is removed from the recipient at the great vessels which are then attached to the donor heart. According to the ACC/AHA guidelines, HT is indicated for patients with NYHA class III or IV HF despite continued medical therapy, MCS use, and surgical management (Yancy et al., 2013). Comorbidities such as irreversible renal failure, liver disease, pulmonary disease, and pulmonary artery

hypertension may be contraindications for HT if a physician believed the conditions would not improve after HT (Hullin, 2014; Yancy et al., 2013). While HT is considered the best-in-care for end-stage HF patients, complications are still common despite a 5-year survival rate of 70% (Alraies & Eckman, 2014). Graft failure is the leading cause of death in the first 30 days after transplant, and infection is the most prevalent complication in the first year after transplant (Lund et al., 2017).

<div align="center">D. <u>Types of Mechanical Circulatory Support</u></div>

MCS use has become increasingly more common in order to relieve HF symptoms and alleviate the growing wait list for HT. MCS systems can be categorized based on duration of care with short term devices including those used primarily in patients experiencing cardiogenic shock and long-term devices serving as more dedicated circulatory support.

Short-term, temporary MCS devices are primarily used to decrease preload and afterload and enhance CO in patients experiencing cardiogenic shock such as from myocardial infarction and in patients undergoing high risk cardiac interventions such as percutaneous coronary interventions and trans-catheter aortic valve implantations (Ferrari et al., 2015; Gilotra & Stevens, 2014). Intra-aortic balloon pumps (IABPs) are used to provide MCS during cardiogenic shock, during high risk procedures, and as a bridge to cardiac surgery. The balloon is placed in the descending aorta usually via the femoral artery and is inflated during diastole then deflated during systole creating a counterpulsation pumping mechanism. This counterpulsation works to enhance LV unloading, decrease preload and afterload, and improve coronary perfusion (Gilotra & Stevens, 2014). The Impella (ABIOMED, Danvers, MA) family of various sized percutaneous ventricular assist

devices (VAD) is an alternative to IABPs for use in high risk cardiac interventions and during cardiogenic shock. The Impella is implanted similar to IABPs through the femoral artery, but its motor assemblies are placed retrograde across the aortic valve into the LV and left in place typically up to 5 days (Sarkar & Kini, 2010). The Impella provides patient support and LV unloading by continuously pumping blood from the LV into the systemic circulation independent of LV contraction and heart rate.

Extracorporeal membrane oxygenation (ECMO) is a form of MCS for HF patients who require acute cardiac support for longer periods than IABPs or Impella devices can provide. In addition, for patients who require respiratory support, ECMO can be utilized to externally oxygenate blood and return it to the circulation. Venovenous (VV) ECMO is used to provide support for patients experiencing respiratory failure. This ECMO circuit removes deoxygenated blood from the inferior vena cava and returns oxygenated blood to the right heart through cannulas placed in the right femoral vein and right jugular vein respectively. For patients who require hemodynamic support in addition to gas exchange, venoarterial (VA) ECMO removes deoxygenated blood from the inferior vena cava and returns retrograde oxygenated blood flow to the aorta. VA ECMO is used to primarily bridge patients to longer term support such as left ventricular assist devices (LVADs) or HT (Gilotra & Stevens, 2014).

Long term MCS for HF patients is provided by the use of VADs or total artificial hearts (TAHs). VADs work to support cardiac output and end-organ perfusion by reducing the myocardial workload. These devices can be used to support the function of both the right (RVADs) and left ventricles (LVADs), however systemic circulatory support is their primary use case. Figure 5 shows the effect that VADs have on the HF PV loop as they

reduce myocardial work and unload the failing ventricle. First generation VADs such as the Thoratec PVAD (Abbott, Chicago, IL) used an internal membrane to displace blood volume by utilizing large external pneumatic drivers and creating pulsatile blood flow (PF). Second generation devices such as the HeartMate II (Abbott) were developed to be smaller and more easily implanted and used internal impellers which deliver continuous blood flow (CF). Current third generation devices such as the HVAD (HeartWare / Medtronic, Framingham, MA) continue to provide CF support, however the internal impeller is levitated by hydrodynamic or magnetic forces which minimizes thrombosis and bearing failure.
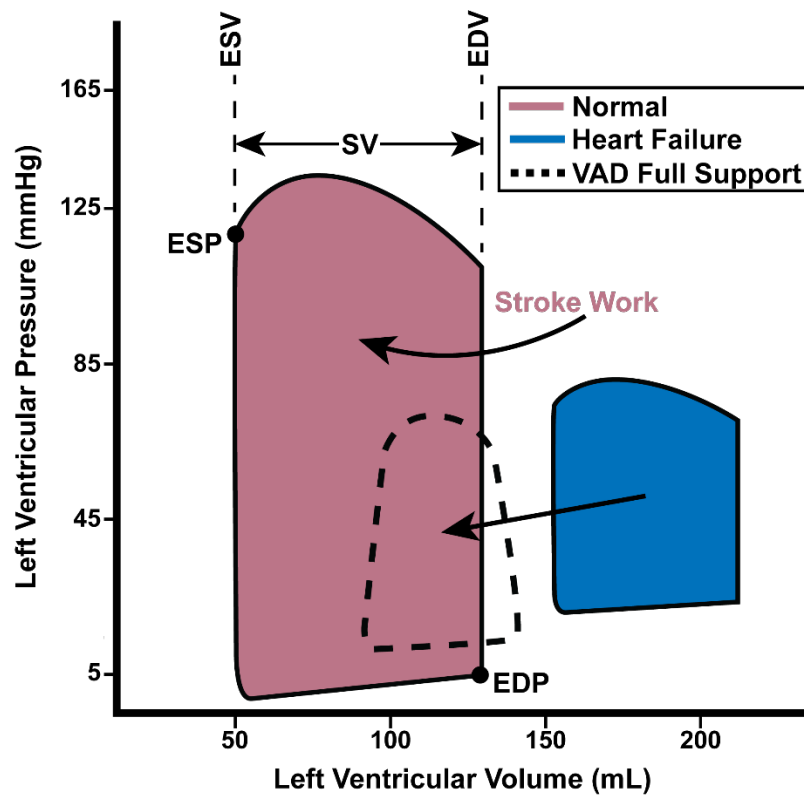
FIGURE 5: Effects on PV relationship due to VAD support. Preload decreases as the ventricle is further unloaded, therefore the PV loop shifts back to the left (blue to dashed line) as the VAD reduces ventricular volumes. The PV loop becomes even smaller due to the reduction in stroke

work as the VAD reduces the myocardial workload. ESV: end-systolic volume; EDV: end-diastolic volume; ESP: end-systolic pressure; EDP: end-diastolic pressure; SV: stroke volume.

While the use of VADs has become increasingly popular to treat late stage HF patients, some of those patients may be too sick to actually benefit from VAD support. However, those patients need to be treated before a HT becomes viable, so a TAH is used to replace their failing heart with a system that can maintain perfusion for the pulmonary and systemic circulations at once. TAHs are implanted by removing the native heart at the atria and sewing the device's atrial cuffs to the remaining atrial tissue. The AbioCor Implantable Replacement Heart (IRH; ABIOMED) was used as an alternative to HT for DT, however it is no longer in clinical use due to high costs and poor outcomes (Ferrari et al., 2015). The SynCardia TAH (TAH-t; Syncardia, Tucson, AZ), formerly known as the CardioWest TAH, is in clinical use for BTT therapy and is currently the only commercially available TAH. In a multicenter study examining the safety and efficacy of the TAH-t in patients eligible for HT with irreversible biventricular failure, 79% of patients survived to transplant compared to only 46% of control patients without a TAH-t implanted (Copeland et al., 2004). In addition, the TAH-t was shown to improve the survival rate post-transplantation with a one-year survival rate of 70% for TAH-t patients compared to only 31% for control patients.

<center>E. <u>Clinical Challenges of VAD Support</u></center>

While VADs have become increasingly beneficial in treating HF patients and reducing the number of patients urgently needing a HT, their use is not without clinical complications. Suction events, right ventricular (RV) failure, bleeding and thrombotic events, infection, and valvular disease are some of the post-implant complications which have been associated with VAD use (Ensminger et al., 2016).

<center>17</center>

RV failure is one of the primary concerns post-VAD implant as it is a significant risk factor for mortality occurring in 10-40% of LVAD patients (Lampert & Teuteberg, 2015). When the RV becomes overloaded with volume compared to the LV, LV filling pressure and volume can decrease and cause a reduction in CO. With increasing decompression of the LV as VAD speed and LV unloading increases, the interventricular septum begins to experience a leftward shift as the septum is pulled towards the LV (A. H. Goldstein et al., 2005). This shift causes the RV to dilate and hinders the septal contribution to RV ejection which can induce right heart dysfunction. RV failure can be treated by lowering VAD speeds until an adequate LV volume can be achieved which can help to reverse the septal shift, or an RVAD can be implanted creating a BiVAD support system where both circulations are perfused by MCS (Potapov et al., 2011; Toda & Sawa, 2015). In addition, RV failure can lead to ventricular arrhythmias which can cause thrombotic events; subsequently, patients should be considered for ICD implant if not previously performed (Potapov et al., 2011).

Infections due to VAD implant are common (13.6 events/100 patient months in first 3 months post-implant) and can manifest at the pump's drive line tunneling site, in the pump's pericardial pocket, and at the outflow graft and apical sewing ring anastomosis which can lead to development of LV endocarditis (Kirklin et al., 2017). If treatment with antibiotics fails to resolve infections, a device replacement or even HT may be the only option (Potapov et al., 2011; Toda & Sawa, 2015). Valvular diseases such as mitral stenosis (MS), mitral regurgitation (MR), aortic insufficiency (AI), and animation problems of the aortic valve, including aortic valve fusion and supra-aortic blood stasis, can occur in VAD patients and are usually treated with valve replacement or by surgically closing the valve

(Adamson et al., 2011). AI can lead to a decreased end-organ perfusion and a reduction in cardiac output if not corrected and may indicate potentially unsuccessful long-term VAD treatment (Potapov et al., 2011).

VAD patients are at an increased risk for bleeding complications post-implant due to the required anticoagulation needed to reduce the chance of pump thrombosis. Bleeding complications have been observed to have a higher incidence in CF-VAD patients, and this has been suggested to be due higher shear stress on blood leading to acquired von Willebrand syndrome (Barić, 2014; Ensminger et al., 2016; Greenwood & Herr, 2014). Despite anticoagulation therapy, patients may still experience pump thrombosis events, and the incidence of thrombosis has been observed to be increased with the use of CF rotary pumps compared to pulsatile devices (D. J. Goldstein et al., 2013). However, the increased incidence may be due to longer support periods that are common with CF-VADs compared to PF-VADs (Ensminger et al., 2016).

These findings have introduced a debate revolving around the need for a physiologic pulse and if these conditions are due to the lack of pulsatile flow. Early studies found that pulsatile flow and pulse pressure was responsible for maintenance of capillary structure, fluid balance, and nutrient exchange (Prior et al., 1995; Takeda, 1960). Bartoli et al showed that pulsatile unloading of the LV in a heart failure bovine model preserved myocardial and vascular energy more than continuous unloading (Bartoli et al., 2010). Studies have found that AI may be linked to a lack of aortic valve opening, and it has been proposed that CF devices prevent the aortic valve from opening during high support because of increased strain on the valve leaflets (Cowger et al., 2010; Hatano et al., 2011; May-Newman et al., 2010). However, Potapov et al could not identify relevant differences between continuous

and pulsatile flow profiles in arterial wall characteristics of clinical samples and concluded that long-term CF-VAD use did not adversely affect vascular wall properties (Potapov et al., 2012). Additionally, Radovancevic et al compared end-organ function in patients on long-term VAD support and concluded based on their data that both CF-VADs and PF-VADs provided adequate end organ perfusion (Radovancevic et al., 2007). Therefore, there is no clear conclusion about the long-term effects of CF-VAD use. Yet, the growing amount of evidence suggesting that these unwanted changes in cardiac physiology may be stimulated by the lack of a physiological pulse has prompted the development of pump speed modulation algorithm with CF devices to provide a more physiologic PF profile.

F. Pseudo-Pulsatile Flow

Various efforts have been made into modifying device operational characteristics of current generation devices to induce pulsatile flow, however these modifications can only achieve a quasi-pulsatile flow instead of true pulsatility due to the always-on nature of the internal impeller. Clinicians have primarily resorted to reducing the speed of CF devices which promotes aortic valve opening, reducing the chance of AI, and allows the heart to promote natural pulsatility by having a greater share of the systemic flow (Bartoli & Atluri, 2015). However, Yang et al tested a transparent replica of a HeartMate II device in a mock circulatory loop and found that operating CF devices in these "pulsatile" conditions can increase turbulent flow within the pumps (Yang et al., 2015). It was suggested that the recent increase in pump thrombosis incidents could be at least partially attributed to the trend of reduced speed CF-VAD use. Therefore, operating these devices at lower speeds is not the complete answer to inducing pulsatile flow, and it has been proposed that CF-VADs

can be programmed to produce near physiologic pulsatility and volume unloading by modulating pump speed (Barić, 2014; Moazami et al., 2015).

One of the earliest studies performed on this topic was Bearnson et al in 1996 who found it was possible to operate a CF device in a pulsatile fashion using a computer model controlling a centrifugal prototype pump in a mock circulatory loop (Bearnson et al., 1996). In an ovine model, Bourque et al in 2006 operated the HeartMate III (Abbott) in a pulsatile fashion by alternating between high and low speed at a rate of 60 bpm which resulted in a pulse pressure of 30 mmHg, yet their quantification of pulsatility did not improve from CF operation (Bourque et al., 2006). More recently, research into strategies to induce pulsatility has focused on synchronizing speed modulation with the cardiac cycle. Pirbodaghi et al showed that in an ovine model synchronized pulsing provided greater pulsatile and physiologic hemodynamics compared to CF (Pirbodaghi et al., 2012).

In addition, various timing strategies for synchronized pulsing such as co-pulsation and counter-pulsation have been developed to investigate potential benefits from different modulation profiles. Co-pulse operation is when the VAD's high speed period occurs during systole and its low speed period occurs during diastole, and the reverse is true for counter-pulse operation. Studies comparing these two strategies have concluded that counter-pulsation increases ventricular unloading while decreasing pulse pressure and myocardial oxygen demand and that co-pulsation increases pulse pressure and myocardial oxygen demand while decreasing ventricular unloading (Moazami et al., 2015; Shi et al., 2010; Umeki et al., 2012; Umeki, Nishimura, Ando, et al., 2013; Umeki, Nishimura, Takewa, et al., 2013). Ising et al used a computational model to test over 150 different speed modulation algorithms and found that asynchronous modulation significantly

increased energy equivalent pressure (EEP) and surplus hemodynamic energy (SHE), which are measures of pulsatility, compared to synchronous algorithms (Ising et al., 2011). The same conclusion was reached by Soucy et al who compared co-pulse, counter-pulse, and asynchronous CF-VAD operation in an ischemic heart failure bovine model (Soucy et al., 2015). It was demonstrated that counter-pulsation reduced LV external work (LVEW) and provided the best support for relieving stress from a failing heart and that co-pulsation generated greater pulsatility while providing the best hemodynamic support in ischemic heart failure animals. However, Soucy et al. concluded that asynchronous modulation demonstrated a greater potential to restore pulsatility compared to synchronous operation, and this could be potentially attributed to intermittent periods of co-pulse and counter-pulse support. Asynchronous modulation also possesses the inherent benefit of not requiring a trigger signal to synchronize the device's rotor to the heartbeat which greatly simplifies its implementation in VADs compared to co-pulse or counter-pulse mechanisms.

G. Technology Overview

Currently, there is little information reported on the long-term physiological effects of speed modulation. In this study, pump and hemodynamic performance of asynchronous modulation were investigated in a chronic healthy bovine model using two CF-VADs providing partial cardiac support: the HeartWare HVAD and a proprietary device VADx.

The HVAD has a centrifugal flow profile with an impeller that is suspended by hydrodynamic and magnetic thrust bearings which prevents impeller contact with the pump housing. The device itself is comprised of three primary parts: a front housing with an integrated inflow cannula, an internal rotor with a wide-blade impeller, and a rear housing with an internal, magnetic center post (LaRose et al., 2010). Both housings contain a motor

stator with six copper coils, and the impeller contains four magnets on its perimeter and a stack of magnets surrounding its center hole. A magnetic force between the center post and impeller maintains radial support and positioning of the impeller towards the front housing. The device's driveline contains motor cables which connect the pump to an external controller which sends electrical signals to the dual motor stators in the pump housings creating an electromagnetic force that rotates the impeller at speeds ranging from 1,800 to 4,000 RPM (LaRose et al., 2010). The driveline is also responsible for supplying power to the device from an external battery pack or DC power supply connected to the external controller. Blood is pulled into the pump through the inflow cannula, pushed to the perimeter of the housing by the impeller blades, and propelled through the outflow graft by the centrifugal force of the impeller rotation.
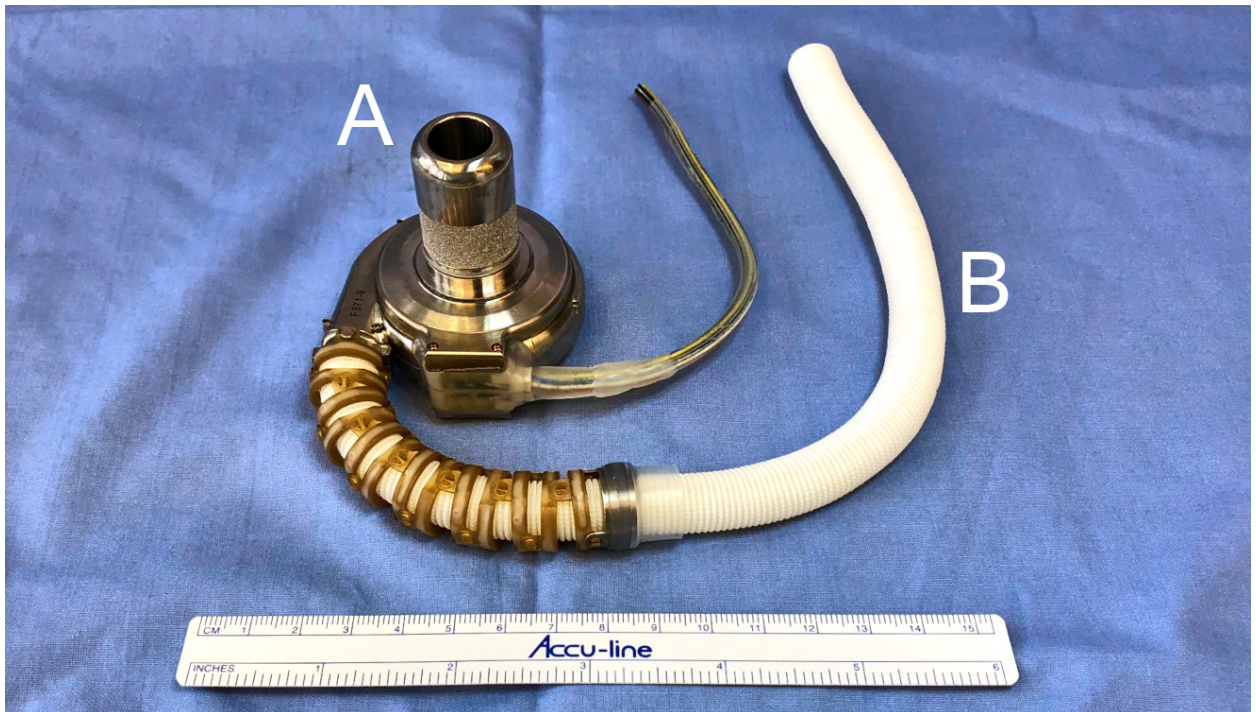
FIGURE 6: The HeartWare HVAD with pump inlet to LV apex (A) and outflow graft to the ascending aorta (B). VADx (not pictured) has its pump inflow placed in LV apex and its outflow cannula tip placed across the aortic valve.

The VADx is an axial flow device that includes a single tubular pump housing wrapped around the impeller and vane diffuser. The device incorporates a base pedestal which is secured to the ventricular apical sewing ring, the pump housing with rotor internals and vane diffuser, a standpipe connecting the pedestal to the pump housing, and an outflow cannula (Slaughter et al., 2011; Tamez et al., 2014). The entire assembly is positioned inside the LV with the outflow cannula crossing the aortic valve. The VADx's impeller is a single piece of metal allowing it to be magnetized as one unit and has hydrodynamic bearings attached to each impeller blade. The standard radial motor stator inside the pump housing is able to create rotational speeds from 12,000 to 22,000 RPM and provides radial stability for the floating impeller that is partially lifted with the hydrodynamic force of blood (Slaughter et al., 2011; Tamez et al., 2014). Blood is pulled in from the bottom of the pump housing past the impeller to the vane diffuser which is responsible for reducing turbulent flow and improving hydraulic efficiency. Blood exits through the outflow cannula which has a trilobar diffuser tip positioned across the aortic valve which provides a radial force component to the blood flow and provides radial stability to the outflow cannula (Slaughter et al., 2011; Tamez et al., 2014). The length of the outflow cannula and standpipe can be adjusted to accommodate various long-axis ventricular lengths.

The rotational speed of both devices (HVAD and VADx) is regulated by external controllers. These controllers adjust the power provided to the motor stators in the pump housing or body to set the rotational speed of the impeller. Further information about pump operation in both continuous and pulsatile flow modes can be found in the Methods section. The devices were asynchronously modulated for 30-days in the healthy bovine model to

test the feasibility of the modulation profile as a possible means of controlling phasic ventricular volume unloading and providing near-physiologic aortic pulsatility.

II. METHODS

A. Study Overview

The overall objective of the study was to determine the feasibility of long-term asynchronous pump speed modulation of continuous flow ventricular assist devices to 1) promote phasic ventricular volume unloading 2) provide greater physiologic aortic pulsatility compared to devices operated at constant speed and 3) minimize risk of additional blood trauma in a partial VAD support model. A chronic 30-day bovine model utilizing healthy, male Jersey calves was selected for this study due to anatomical similarities with the human thoracic and cardiovascular systems as described in Monreal et al. (Monreal et al., 2014). This study was conducted in accordance with the National Institutes of Health Guidelines for the Care and Use of Animals in Research (National Research Council (US) Committee for the Update of the Guide for the Care and Use of Laboratory Animals, 2011), and all experimental procedures were approved by the Institutional Animal Care and Use Committee (IACUC) at the University of Louisville.

B. Experimental Design

A chronic bovine model consisting of healthy, male Jersey calves was used to investigate the clinical effects of asynchronous speed modulation of two different ventricular assist devices: the HeartWare HVAD (n=3 animals) and a proprietary device

VADx (n=4 animals). Animals were quarantined for a minimum of 14 days upon arrival after which they underwent an implantation procedure for their respective devices. The study was carried out for 30 days to investigate any hemodynamic and physiologic changes that could be caused by asynchronous modulation. At day-30 post-implant, the animals underwent a terminal fluoroscopy procedure then euthanized and transferred to the necropsy room for gross dissection. Both devices were tested in continuous flow (CF) and pulsatile flow (PF) mode during the implant and day-30 terminal procedures and were operated in PF mode during the study period.

<div align="center">C. <u>Experimental Procedures</u></div>

1. <u>Implantation</u>

Healthy, male Jersey calves (n=7) weighing 52±3 kg upon arrival were quarantined for a minimum of 14 days during which veterinarian assessment were performed, and the calves were treated with preventative medicine as follows. Animals implanted with a VADx device were administered CORID 20% Soluble Powder (50mg/kg PO) to treat and prevent coccidiosis and Panacur (50 mg/kg PO) to remove and control lungworms, stomach worms, and intestinal worms. Animals implanted with an HVAD device were administered Banamine (2.2 mg/kg IV) for pain management, Excede (6.6 mg/kg SQ) for antibiotic treatment, and a probiotic (15 mL PO) to promote healthy bacterial growth.

After quarantine, calves were prepared for the implantation procedure as follows. On the day prior to surgery, a transdermal 25 or 50 mcg/hr fentanyl patch was applied to the animal's flank for calves weighing less than or equal to 80 kg and greater than 80 kg, respectively. A venous blood sample was collected from the jugular vein for baseline complete blood count (CBC), biochemical analysis, and coagulation status. The calf was

weighed to obtain its pre-fasting weight, and fasting of solid food began 18-20 hours prior to the scheduled time of surgery the next morning. Water was withheld 3-4 hours prior to surgery.

On the morning of surgery, the calf was first weighed to obtain its fasting weight. Induction of anesthesia was achieved by intravenous (IV) administration of a ketamine (4 mg/kg; for dissociative sedation) and diazepam (0.4 mg/kg; for anxiolysis) mix for the implantation procedure. The calf was then intubated, and anesthesia was maintained with isoflurane at 1-5% with oxygen saturation maintained above 90% for the duration of the procedure. An intravenous catheter was placed in a marginal ear vein for administration of IV infusions prior to central line placement. IV infusions included carrier fluids of Lactated Ringer's Solution (LRS) or Normosol-R (50-200 mL/hr), amiodarone (1.8 mg/mL at 17-25 mL/hr) to control arrhythmias, dobutamine (3-5 mcg/kg/min) to control blood pressure, and fentanyl (1-10 mcg/kg/hr) for pain management. Electrocardiography (ECG) electrodes were sutured onto the skin for lead-II intra- and post-operative monitoring of normal cardiac electrical activity, and a pulse oximeter was attached to the ear for intra-operative monitoring of blood oxygenation levels. Additionally, placement of an orogastric (OG) tube was used to decompress the animal's rumen during surgery. Transesophageal echocardiography (TEE; X7-2t probe and iE33 portable ultrasound machine, Phillips, Amsterdam, Netherlands) was used for intraoperative cardiac monitoring, data collection, and to assist with device placement.

In the operating room (for HVAD animals) or fluoroscopy room (for VADx animals), sterile technique was used for the implantation procedure. Cefazolin (15-20 mg/kg IV), fluxinin meglumine (1.1-2.2 mg/kg IV), and magnesium sulfate (2 g over 1-hour IV) were

administered for antibiotic prophylaxis, pain management, and arrhythmia control, respectively. For the implantation procedure, the calf was first placed in a right lateral recumbency position where the calf's right neck was cleaned, prepped, and draped in sterile fashion, and the right jugular vein was isolated for vascular access port (VAP) insertion (9Fr VAP, Norfolk Medical, Skokie, IL). A separate pocket under the subcutaneous tissue was made for the VAP which was secured to the underlying fascia and the neck closed with 2-0 Vicryl suture. The calf was then repositioned to a left lateral recumbency position where the calf's left neck and chest were cleaned, prepped, and draped in sterile fashion. The left jugular vein and carotid artery were accessed via a surgical cutdown. A 7Fr triple lumen catheter (Mila International, Florence, KY) was placed in the left jugular vein via Seldinger technique to monitor central venous pressure (CVP) and serve as the central venous line for IV infusions. A 7Fr introducer sheath with sidearm (Argon, Frisco, TX) was placed in the left carotid artery to monitor arterial pressure (ART), to obtain arterial blood samples, and for catheter access to the LV.

During the implant procedure, succinylcholine (30mg bolus IV) and lidocaine (100mg bolus IV) were administered as needed for neuromuscular blockade and cardiac arrhythmia control. Intraoperative arterial and venous blood samples were collected every 30 minutes for oximetry and chemistry monitoring using a portable blood analysis device (i-STAT 1, Abbott, Lake Bluff, IL). Blood samples were also used to measure activated clotting time (ACT) with an ACT-II device (Medtronic, Minneapolis, MN) to monitor coagulation status. Baseline TEE data, including structural and functional parameters, was collected prior to device implantation. Hemodynamic measurements throughout the study were recorded with respiratory suspended at a sampling rate of 400 Hz using a PowerLab 16/35

module (ADInstruments, Sydney, Australia) connected to the LabChart data acquisition software (version 8, ADInstruments).

a. <u>HVAD Implantation</u>.   The HVAD device was first prepared by following the clinical instructions for use provided by HeartWare. Briefly, the device was submerged in a 5% dextrose solution for the initial pre-implant pump test run lasting 30-60 seconds at 1800 RPM. Afterwards, the outflow graft and strain relief were attached to the device's outflow conduit. De-airing of the pump before implant was achieved by filling the assembly with a saline solution.

Via a left thoracotomy approach, an approximately 14cm chest incision was made over the 5th rib which was subsequently removed. The pericardium was opened anterior to the phrenic nerve, and the ascending and descending aorta were exposed. A 24-28 mm flow probe (Transonic, Ithaca, NY) was placed on the ascending aorta to measure aortic root flow (AoF), and its cable was tunneled through the skin to exit towards the spine. Baseline hemodynamics including arterial and central venous pressure and AoF were then recorded prior to pump implantation.

After baseline hemodynamics were recorded, the pump drive line was tunneled under the skin to exit towards the spine. Heparin (10,000 units IV) was administered to maintain an ACT greater than 480 seconds. After heparinization, the outflow graft was cut to size and anastomosed to the descending aorta using running 3-0 polypropylene suture. The apex of the LV was elevated and exposed, and the HVAD apical sewing ring was sutured on using 8 interrupted, pledgeted 2-0 Ethibond sutures. The apical coring device was used to create a hole for the inflow cannula of the pump which was inserted and secured to the apical ring. A 10 mm flow probe (Transonic) was then placed on the VAD outflow graft to

measure VAD flow (VADF), and its cable was tunneled through the skin and to exit towards the spine.

The heart was then lowered, and the device was turned on and operated as described in the Pump Operation section. The device was tested in CF and PF modes during which hemodynamic and TEE data were recorded with ventilation suspended (at end-exhalation) in 30 second epochs. A 28Fr chest tube was placed in the chest cavity then tunneled through the skin to exit towards the ventral side of the abdominal region and connected to a water seal chest drain. The chest was closed with 0 and 2-0 Vicryl suture.

The triple lumen catheter in the left jugular vein and introducer sheath in the left carotid artery were exchanged for temporary IV lines prior to transporting the calf to the post-operative care room. The left neck was closed using 2-0 Vicryl and 2-0 nylon sutures. The temporary lines were secured with 2-0 nylon suture and left in place for an average of 16 days during the study and then removed once the animals no longer required intravenous infusions and medication. After central line removal, the VAP was used to administer IV medications as needed as described in the Post-Operative Care section.

An intercostal nerve block was performed (Exparel, 2 mg/kg) for pain management at the thoracotomy site. Field blocks (Exparel) were performed at the thoracotomy site, all exit sites, and both the left and right neck incisions. Finally, the calf was transferred to the post-operative care room, weaned from general anesthesia, and extubated.

b. VADx Implantation. In contrast to the HVAD, the VADx device does not need to be assembled in the operating room. Preparation of the device in the fluoroscopy room began with an initial test run in 5% dextrose solution lasting for at least one minute. A 7Fr

Swan-Ganz balloon catheter (Edwards Lifesciences, Irvine, CA) was placed through the device's pedestal and inflated in the pump body for de-airing during implantation.

Via a left thoracotomy approach, an approximately 10cm chest incision was made over the 5th rib which was subsequently removed. Heparin (10,000 units IV) was administered to maintain an ACT greater than 480 seconds. The pump drive line was tunneled under the skin to exit towards the spine, and the heart was elevated to expose the left ventricular apex. The VADx sewing ring was secured to the apex with interrupted 2-0 pledgeted Ethibond sutures. The apical coring device was used to create a hole within the sewing ring through which the VADx was inserted. The device's outflow cannula was placed across the aortic valve under echocardiographic guidance, with position confirmed by fluoroscopy. De-airing of the VADx was achieved through continuous flushing of the balloon catheter until the cannula was inside the ventricle. Once the cannula crossed the aortic valve, the balloon catheter was deflated and retracted. Retrograde blood flow through the base of the pedestal was prevented by an internal one-way valve before the locking pin was secured in the pedestal's cavity. For VADx animals during the implant procedure, phenylephrine (100-300 mcg bolus) and protamine (3-4 mg/kg IV) were administered as needed to treat hypotension and reverse the effects of heparin.

The heart was lowered, and the pump was turned on and operated as described in the Pump Operation section. A pressure-volume catheter (Millar, Houston, TX) was introduced into the LV through the carotid artery introducer sheath for data collection during the implant procedure. The device was tested in CF and PF modes during which hemodynamic and echocardiographic data was recorded with ventilation suspended (at end-exhalation) in 30 second epochs. The remainder of the procedure was performed as

previously described in the HVAD implantation section beginning with placement of the chest tube. The pressure-volume catheter was removed before closure of the chest and left neck.

2. Post-operative Care

During post-operative care, animals were monitored continuously by veterinary personnel. Arterial and venous blood samples were tested for blood oximetry and chemistry every hour for the first 48 hours then as needed using the i-STAT device. The ACT-II was used to assess ACT every 4 hours until stable then every 6 hours. In addition, arterial blood samples were collected to assess CBC (Hemavet 950, Drew Scientific, Miami Lakes, FL) and plasma free hemoglobin (pfHb; HemoCue Plasma/Low Hb Photometer, Brea, CA). Blood samples were sent to the University of Louisville Hospital for analysis of prothrombin time/international normalized ratio (PT/INR). CBC and pfHb tests were performed at 1, 8, 16, and 24 hours post-operatively, and PT/INR testing was done daily for the first week then twice weekly. Animals were removed from their holding pens weekly to be walked on a treadmill for 10-15 minutes for exercise.

IV infusions were continued from the implant procedure into the post-operative care room. Dobutamine infusion was discontinued before transport from the implant procedure, and amiodarone and fentanyl infusions were weaned off 4 days post-implant. Heparin infusion (200-300 units/kg IV; 1000 units/mL at 5 mL/hr initially) was administered as needed to prevent thrombus formation and maintain an ACT of 200-300 seconds. Potassium chloride (in 0.9% saline at 0.5 mEq/kg/hr) and nicardipine (1 mg/mL at 5-20 mg/hr IV) infusions were administered for the first three days post-implant to treat hypokalemia and hypertension respectively. Cefazolin (15-20 mg/kg IV) was administered

two to three times daily for 7-14 days post-implant to prevent infection, and flunixin meglumine (1.1-2.2 mg/kg IV) was administered 72 hours post-implant for post-operative analgesia. Warfarin (5-10 mg titrated in 2.5 mg increments PO) was administered to maintain an INR of 1.5-2 times the animal's baseline through the study duration. Atenolol (100 mg IV) was given up to three times daily for the study duration to manage blood pressure.

All HVAD and VADx devices were operated in PF mode during post-operative care according to the device operation sections. Hemodynamic measurements consisting of ART, CVP, AoF, and VADF for HVAD animals and ART and CVP only for VADx animals were recorded for five-minute epochs at the beginning of every hour for the study duration until the arterial and central venous lines were removed.

3. 30-day Terminal Study and Necropsy

At day-30 post-implant, the animals were taken to the fluoroscopy room for their terminal procedure. The animals were anesthetized with propofol (4-6 mg/kg IV) via the VAP, intubated, and prepped for surgery as previously described for the implant procedure. During the terminal procedure, lidocaine (100 mg bolus IV) was administered as needed to control cardiac arrhythmias. The animal was placed in a left lateral recumbency where a 5 cm incision was made on the left neck over the jugular vein and carotid artery. Both vessels were isolated, and a 7Fr triple lumen catheter (Mila International) was placed in the jugular vein for pressure monitoring. A 7Fr introducer sheath with sidearm (Argon) was placed in the carotid artery for pressure monitoring and ventricular access. A ventriculography catheter was passed into the carotid introducer sheath, retrograde across the aortic valve, and into the LV. Contrast (Conray-43) ventriculography (INNOVA 3100

Fluoroscopy Unit, GE Healthcare, Chicago, IL) was performed to assess ventricular size, device flow, and presence of mitral or aortic regurgitation. For animals implanted with an HVAD, a pressure-volume catheter (Millar) was passed through the introducer sheath to measure left ventricular pressure (LVP) and volume (LVV). For animals implanted with the VADx device, a pressure-only catheter was instead used to measure LVP only, and an additional pressure catheter was used to measure aortic pressure (AoP).

Terminal hemodynamic data for CF, PF, and VAD off conditions were recorded including ART, CVP, and LVP and LVV for HVAD animals or LVP and AoP for VADx animals. Refer to the Pump Operation section for further details. In addition, terminal TEE data was recorded for each condition, and fluoroscopic images were recorded to ensure there was no blockage of VAD inflow or outflow grafts/cannulas. All hemodynamic and TEE data was collected with ventilation suspended (at end-exhalation) in 30 second epochs. After terminal data was recorded, at least 30,000 units of heparin were administered intravenously to achieve an ACT greater than 480 seconds to ensure no blood clot formation would occur in the body or VAD before dissection. The calf was euthanized with an IV bolus of Beuthanasia-D (0.1 mL/lb. IV) and transferred to the necropsy room. The veterinarian completed a gross examination, and the pump was carefully removed from the calf and examined for any sign of thrombus or malfunction.

D. Pump Operation

1. HVAD Operation

HVAD devices were controlled by the Clinical Data Acquisition System (CDAS) software developed by HeartWare, Inc. The software was able to operate the device in CF or PF modes. CF was set by the speed of the internal rotor in RPM. PF was determined by

setting the maximum speed in RPM, the percentage drop to the minimum speed, and the time for high and low speed duration (setting the duty cycle). When the HVAD devices were operated in PF mode, a time of 1.5 seconds was used for the high and low speed periods, effectively setting the duty cycle at 3 seconds or 20 beats per minute (BPM). Device data including voltage, current, and speed was outputted throughout the entire study duration by the CDAS software and recorded simultaneously with hemodynamic data.

During the implant and 30-day terminal procedures, three operational modes were tested and data recorded: baseline or VAD off, CF mode, and PF mode. For CF, the two HVAD devices were set to 2900 RPM and 3200 RPM. For PF, the same devices were set to a maximum of 3400 RPM with a 20% speed drop and a maximum of 4000 RPM with a 40% speed drop respectively. During post-operative care, the devices were operated in PF and the CDAS software was set to a maximum speed of 4000 RPM with an average speed drop percentage of 37±0.25%. Due to limitations of the CDAS software and hardware interface, if a device is disconnected from CDAS it is possible for it to become fixed at the RPM set directly before disconnection. In consideration of this limitation, the devices were set to CF before the animals were moved for weekly exercise.

2. VADx Operation

VADx devices were controlled by proprietary controller software which was developed in order to operate the devices in either CF or PF modes. CF was set by the speed of the internal rotor of the device in RPM. In contrast to the HVAD devices, PF was determined by setting the maximum speed in RPM, the total drop to minimum speed in RPM, and the duration for high and low speed periods. As in HVAD operation, a time of 1.5 seconds was used for the high and low speed periods. Device data including voltage,

current, power, and speed was outputted throughout the entire study duration by the controller software and recorded simultaneously with hemodynamic data.

Similar to the HVAD devices, three operational modes were tested and data recorded during the implant and 30-day terminal procedures: baseline or VAD off, CF mode, and PF mode. For CF, three VADx devices were set to 15,000 RPM and one device was set to 16,000 RPM. For PF, these devices were set to a maximum of 18,000 RPM with a 6000 RPM speed drop and a maximum of 19,000 RPM with a 6000 RPM speed drop respectively.

During post-operative care, the VADx devices were set to pulsatile operation and the controller software was set to an average maximum of 17510±93 RPM with an average speed drop of 5761±85 RPM. Akin to the CDAS software, a limitation of the VADx controller software and hardware interface fixes the pump at the RPM setting sent to the device directly before it is disconnected from the software. Due to this limitation, the VADx devices were set to CF before the animals were moved for weekly exercise.

E. Experimental Measurements

Unfiltered hemodynamic measurements were recorded throughout the study duration as previously described at a 400 Hz sampling rate. Briefly, for VADx animals, ART, CVP, LVP, and LVV were recorded during implant, ART and CVP were recorded during post-operative care, and ART, CVP, LVP, and AoP were recorded during the terminal procedure. For HVAD animals, ART, CVP, AoF, and VADF were recorded during the implant procedure, post-operative care period, and the terminal procedure. LVP and LVV were additionally recorded for HVAD animals during the terminal procedure. Hemodynamics were used to calculate measures of pulsatility, namely pulse pressure (ΔP),

37

surplus hemodynamic energy (SHE), and arterial impedance (ZART), and determine the effects of each VAD operating condition (no VAD/VAD off, CF, PF) on the waveforms. A summary of data collection is shown in Figure 7 below.
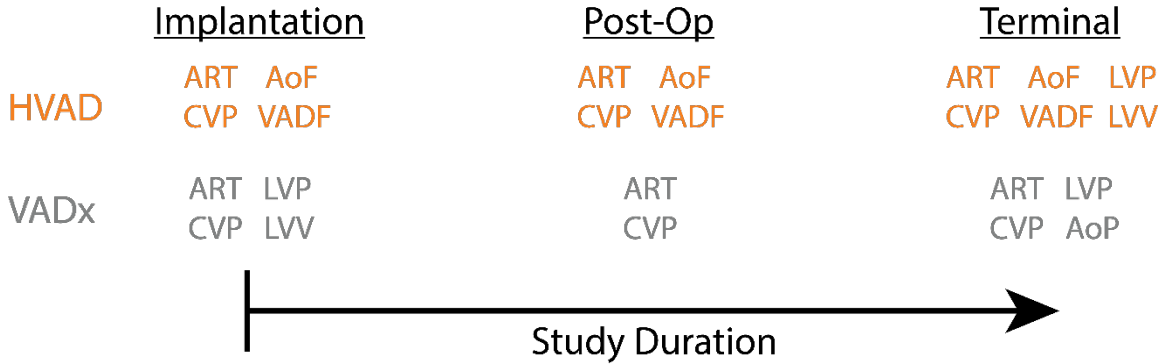
FIGURE 7: Data collection timeline for the full study duration. HVAD animals (orange) were instrumented with flow probes for aortic and VAD flow for the full study duration and with a pressure-volume catheter during the terminal study. LVP and LVV were collected for VADx animals (grey) during the implantation procedure, and LVP and AoP signals were collected during the terminal study.

SHE is calculated using the MAP and energy equivalent pressure (EEP) and is a measure of the extra energy generated by pulsatile blood flow. EEP is a measure of the energy contained in a given volume of fluid pumped through a vessel. The formulas for calculating EEP and SHE can be found in Equations 1 and 2, respectively.

$$EEP = \frac{\int (flow * pressure) dt}{\int flow * dt} \tag{1}$$

$$SHE(ergs/cm^3) = 1332 * (EEP - MAP) \tag{2}$$

ZART is defined as the ratio between the frequency components of the blood pressure and flow waveforms and can be used to study the load on the heart due to vessel characteristics

such as resistance, compliance, and inductance. Example phase and magnitude graphs for

ZART in a healthy bovine heart are shown in Figure 8.
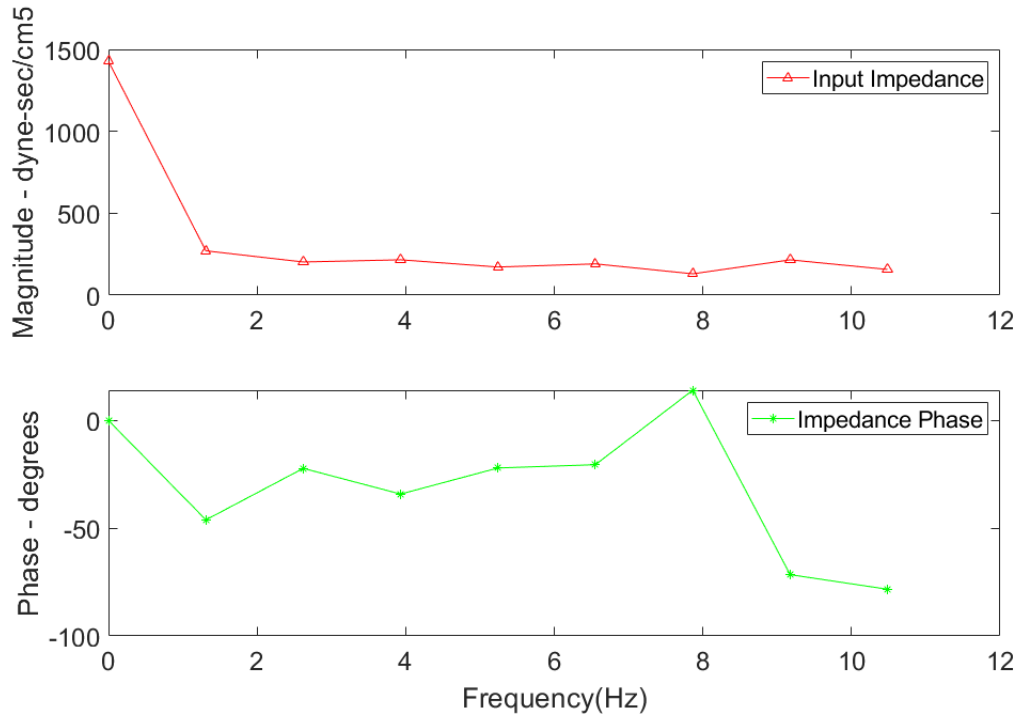
FIGURE 8: Example magnitude and phase plots for ZART. Arterial impedance (ZART) is the ratio between the frequency components of blood pressure and flow and can be split into its magnitude and phase components. The 0th harmonic represents arterial resistance of the vasculature. The negative phase in the first few harmonics indicate normal vascular compliance.

Intrinsic pump parameters including power and speed were recorded as previously described. Briefly, the custom HeartWare VAD controller software (CDAS for HVAD devices or the proprietary software for VADx devices) outputted pump data to comma separated value (CSV) files at set intervals. These data were used to analyze the efficiency of the HVAD and VADx devices in CF and PF modes. Additionally, the data were used to correlate with trends in hemodynamics collected during the post-operative care period.

Echocardiography was recorded as previously described during the implant and terminal procedures. Briefly, TEE was used to capture 3D images of the heart for each test condition of the pumps: baseline or VAD off, CF, and PF. These images were used to calculate stroke volume (SV), cardiac output (CO), ejection fraction (EF), stroke work, and total cardiac work.

Blood oximetry and chemistry, CBC, and PT/INR were measured and recorded as previously described to guide post-operative care and ensure no abnormal events were occurring in individual animals. Blood oximetry results included measurements of lactate, pH, total carbon dioxide (TCO_2), bicarbonate (HCO_3), base excess, oxygen saturation (sO_2), and partial pressures of carbon dioxide (PCO_2) and oxygen (PO_2). Blood chemistry results included measurements of sodium, potassium, chloride, ionized calcium, TCO_2, glucose, blood urea nitrogen (BUN), creatinine, hematocrit, and hemoglobin. ACT results were used to ensure animals were within range (200-300 seconds) to prevent thrombus formation, and pfHb measurements were used to monitor the possibility of thrombus formation and results were correlated with device data.

F. Data Analysis

Echocardiographic images comprised of the apical four-chamber view, the apical two-chamber view, and the short-axis mid-papillary view were analyzed with QLAB software (version 10.2, Phillips, Amsterdam, Netherlands) using the 3DQ or 3DQ Advanced analysis features. 3DQ Advanced was the preferred method of analysis wherein the end-diastolic (ED) and end-systolic (ES) frames were selected, and 10 reference points were set for each frame to determine the border of the LV. For the ED and ES reference points, the septal wall, lateral wall, and apex were chosen on the apical four chamber view, while

the anterior and inferior walls were selected on the apical two chamber view. The short-axis view was used to determine the correct position for the planes of the other two views. The software then calculated the border of the LV for each frame of the cardiac cycle and determined the ED and ES volumes, SV, and EF.

If an advanced 3D image was not captured, 3DQ analysis had to be utilized instead. This method utilized selecting points to the left and right of the mitral valve and the apex of the LV to determine a rough border for the ED and ES frames. The software then calculated the difference in size between the two frames to determine the SV and EF. The results of these analyses were then used to calculate cardiac output using the heart rate at the time of recording, and stroke work and cardiac work using the MAP at the time of recording. Finally, SV, CO, EF, stroke work, and cardiac work were normalized to the weight of the animal at the time of recording.

Hemodynamic waveforms were exported from the LabChart software into tab delimited text files. These data files were loaded into the custom Hemodynamic Estimation and Analysis Tool (HEART) Matlab (version R2016, Mathworks, Natick, MA) software (Schroeder et al., 2004). The HEART software was used to select individual beats to reduce the waveforms into numerical data such as pressure averages and peaks that could then be analyzed further. Once the data files were loaded into HEART and the various signals in the files identified (e.g. AoP, CVP, AoF, etc.), the beats were picked by determining the reference signal (LVP or AoP) and threshold values used in the beat-picking algorithm to determine when the next beat occurred.

For recordings that did not have a true AoP catheter and signal, the ART signal was used to approximate the AoP waveform. Beats were picked on the AoP waveform for all

files to simplify later analysis. Once a recording's beat boundaries were determined, a MAT-file was exported from HEART containing all signals and the AoP beat boundaries. The MAT-files were trimmed at the beginning and end resulting in uniform 30 second epochs for analysis. A custom Matlab script was written to use the beat boundaries to calculate beat-to-beat parameters for each signal such as averages and peaks and calculated values which used multiple data signals such as SHE and ZART. Calculated parameters were outputted for later analysis.

Pump data was imported into Excel (Microsoft, Redmond, WA) for preliminary organization and analysis. For data recorded during the implant procedure, CF and PF data was parsed into 30 second epochs. Mean speed and power was calculated using the average of the data, and peak power was calculated as the maximum power in the 30 second period. To characterize pump efficiency, the percent change from mean speed during PF operation was calculated using the averages of the high and low speed periods to negate overshoot caused by the internal pump control system. Percent change of power usage was calculated using the percent difference between the mean power of CF and PF mode.

Pump data collected during the post-implant period was parsed into 30 second epochs and analyzed by a custom Matlab script which determined the average, maximum, and minimum speed and the average and peak power for each file. Data were transferred to Excel and the percent errors for the speed values from the expected values was calculated.

All hemodynamic, echocardiographic, pump, and bloodwork data were transferred to GraphPad Prism (version 7, GraphPad, La Jolla, CA) for statistical analysis. Hemodynamic and pump data and blood oximetry and chemistry results collected during the post-implant period were used to output trend graphs and averages throughout the study. Plasma free

hemoglobin results obtained during the post-implant period were additionally used to output trend graphs for correlation with hemodynamic and pump results. Statistical analysis was performed to determine significant differences between pump operating conditions during the implant and terminal procedures. For echocardiographic data, Friedman tests, the non-parametric equivalent to repeated measures ANOVA testing, were performed to determine significant differences between the three pump operating conditions: baseline or VAD off, CF, and PF. For comparisons found to be statistically significant, Dunn's post-test was used to determine which operating conditions produced significantly different results. These tests were also used to assess statistical significance in HVAD hemodynamic data. For VADx hemodynamic data, some test conditions could not be analyzed in repeated measures testing due to complications in data acquisition during the surgical procedures. For this reason, unpaired Kruskal-Wallis tests were used to assess significant differences between pump operating conditions, and Dunn's post-test was used to determine which specific operating conditions produced significantly different results. Data is reported as mean ± standard error of the mean (SEM). A value of $p < 0.05$ was considered statistically significant.

III. <u>RESULTS</u>

A. <u>Study Results</u>

This study was carried out to investigate the chronic effects of asynchronous speed modulation of rotary blood pumps on phasic ventricular volume unloading and greater physiologic aortic pulsatility compared to devices operated at constant speed. Two HVAD and four VADx animals achieved the 30-day study endpoint. Due to surgical complications, one HVAD animal died intraoperatively. Both HVAD devices maintained asynchronous modulation for the full study duration. VADx devices maintained asynchronous modulation throughout the study with the exception of two devices that were briefly operated in continuous mode for one and two-day periods. Near-physiologic aortic pulse pressure (ΔP = systolic AoP – diastolic AoP) of 45 ± 4 mmHg and 46 ± 9 mmHg was achieved with asynchronous modulation for HVAD and VADx devices, respectively. In addition, stroke volume was acutely reduced by 23% in HVAD animals from continuous to pulsatile mode. In VADx animals, stroke volume was reduced by 27% in pulsatile operation compared to baseline with no VAD. Plasma-free hemoglobin was maintained within normal limits for all animals with the exception of one VADx animal which experienced a brief spike in pfHb that resolved itself.

B. Operational Device Settings and Intrinsic Pump Parameters

Asynchronous, pulsatile modulation was successfully maintained for the full study duration for both HVAD devices with average high and low speeds of 4000 RPM and 2500 RPM respectively. Two out of four VADx devices successfully maintained synchronous modulation for the study duration with average high and low speeds of 17,289 RPM and 11,764 RPM. One VADx device, implanted in animal #5914, was operated at fixed pump speed for one day due to high pfHb results and risk of thrombosis. The device was restored to asynchronous modulation the next day at its previous settings but later lowered to operational high and low speeds of 14,000 RPMs and 9000 RPM, respectively. The other VADx device was operated at fixed pump speed for two days due to an unforeseen controller malfunction which was corrected to restore asynchronous modulation.
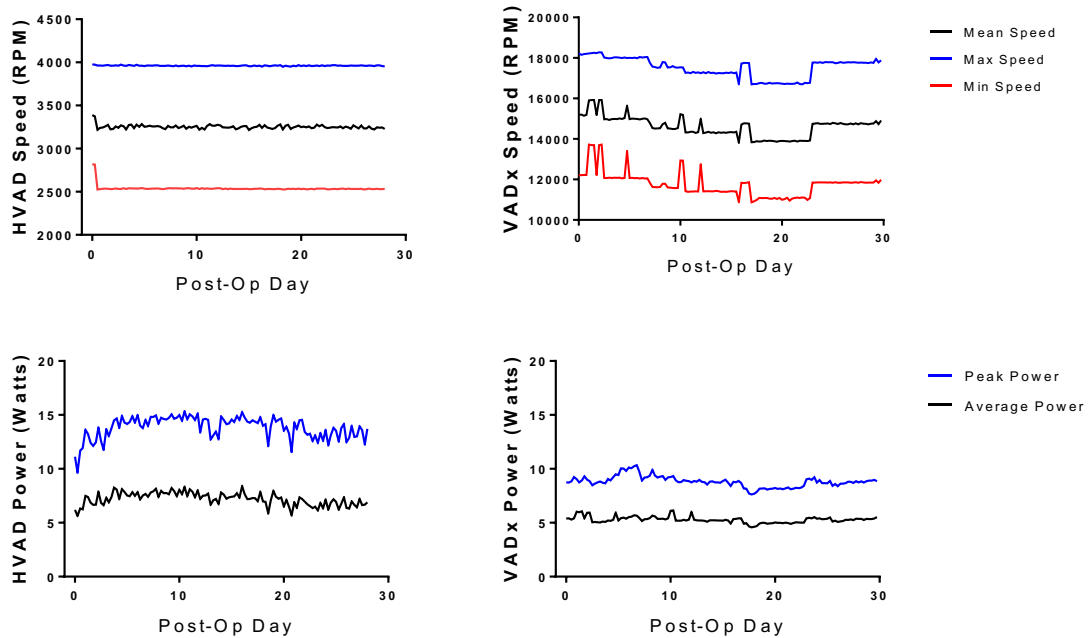
FIGURE 9: Average daily post-operative device power usage and operating speed for HVAD and VADx devices. VADx device operation was varied throughout the study duration due to complications in two of the devices. HVAD and VADx mean power usage was 7.2 ± 0.1 Watts and 5.3 ± 0.0 Watts, respectively. Peak power was 91% larger than average power use for HVAD devices and 67% larger in VADx devices.

HVAD devices were operated at a set maximum speed of 4000 RPM (common clinical therapeutic setting) with an average set speed drop of 37.3% ± 0.1% throughout the post-operative care period. The average power usage throughout this period was 7.2 ± 0.1 Watts with an average peak power usage of 13.8 ± 0.1 Watts. Peak power usage occurred when the devices were ramping up to maximum speed. However, during this speed increase, the HVAD briefly spikes in power usage before settling at its peak power. This spike was an average of 20.36 ± 0.1 Watts during the post-operative care period. VADx devices were operated at an average set maximum speed of 17,263 ± 44 RPM with an average set speed drop of 5794 ± 36 RPM throughout the study duration. Average power

and peak power usage for VADx devices during the post-operative care period was lower than HVAD devices with 5.3 ± 0.0 Watts and 8.8 ± 0.0 Watts respectively. Similar to the HVAD devices, VADx peak power occurred during the device ramp up to maximum speed. No power spike was observed in VADx devices during the speed increase, but this may be due to a low sampling frequency of the controller software. Average post-operative values for analyzed intrinsic pump parameters for both devices can be found in Table II presented as mean $\pm$ SEM (% Error). The percent error for the device speed parameters was calculated using the expected values based on the device set points. HVAD devices were found to have significantly different ($p < 0.0001$) power usage during the post-operative care period from each other.

TABLE II

AVERAGE POST-OPERATIVE INTRINSIC PUMP PARAMETERS

	Median Speed (RPM)	Maximum Speed (RPM)	Minimum Speed (RPM)	Power Usage (Watts)	Peak Power Usage (Watts)
HVAD	3253 ± 2 (0.56%)	3961 ± 0 (0.96%)	2539 ± 4 (1.36%)	7.2 ± 0.1	13.8 ± 0.1
VADX	14602 ± 46 (1.68%)	17522 ± 45 (1.50%)	11752 ± 56 (2.96%)	5.3 ± 0.0	8.8 ± 0.0

Average operating parameters during the post-operative care period. Percentages indicate the percent error that the result is from the expected value based on pump settings. All results expressed as mean $\pm$ standard error of the mean.

1. <u>Device Power and Speed Modulation</u>

During the implantation procedure, the power usage for both devices and the relationship between power and output speed was characterized. The power usage was analyzed in CF mode at a set pump speed and with asynchronous modulation in PF mode. The set operational speeds for the pulsatile modulation were determined so that the median speed matched the CF mode's set mean pump speed. Power usage between the two modes

was compared. One HVAD device experienced a controller malfunction during the testing procedure and was unable to be set to pulsatile settings matching the CF mode. In Figure 10, it can be seen that pulsatile modulation resulted in increased average and peak power usage for both devices. One HVAD device could not be included in the implantation results due to controller malfunctions. Average and peak power usage was higher in both devices when operated in PF mode compared to CF mode during the implantation and terminal procedures. At implantation, peak power usage increased by 74% in one HVAD device and 56% in the VADx devices compared to CF mode. Power usage was reduced at terminal procedure compared to implantation due to lower operational speeds tested.
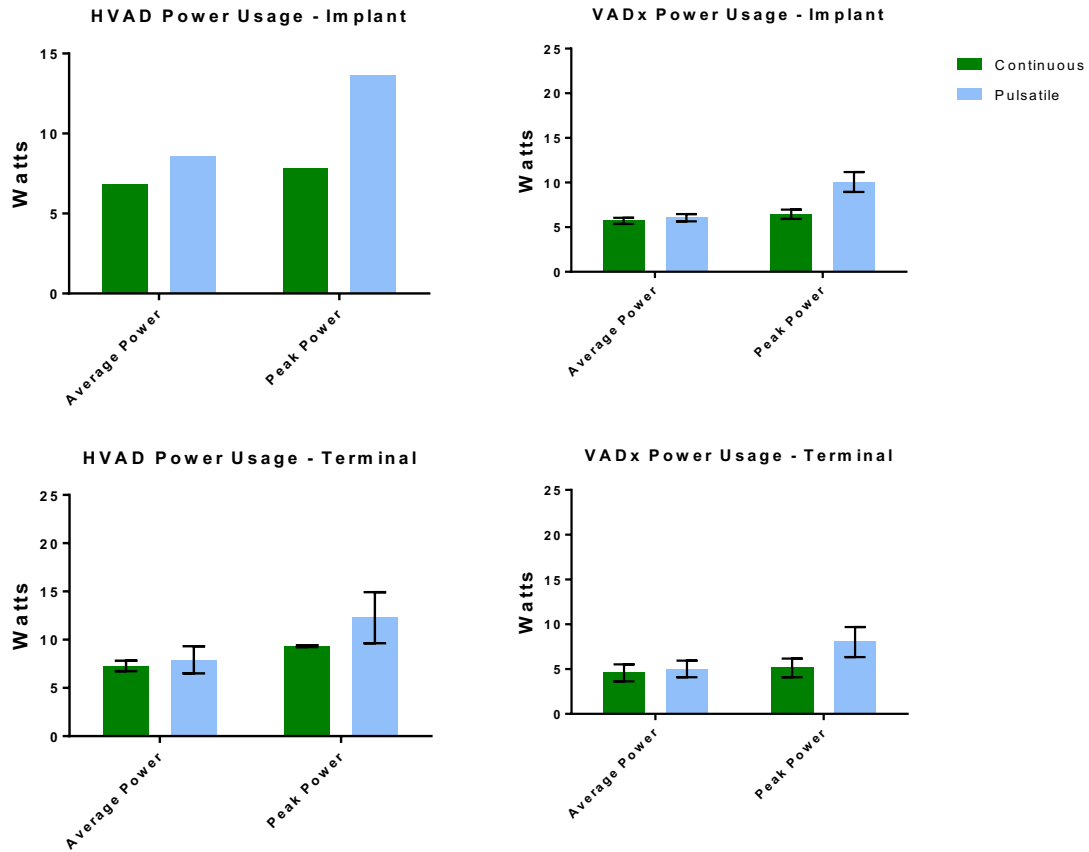
FIGURE 10: Device power usage during continuous and pulsatile flow modes. Asynchronous pulsatile modulation resulted in increased power usage for both HVAD and VADx devices with peak power usage at implant increasing by 74% in one HVAD device and 56% in the VADx devices compared to CF mode. Power usage was reduced at terminal procedure compared to implantation due to lower operational speeds tested. Data is presented as the mean +/- SEM.

The percent change in power usage that occurs to produce a given speed modulation around the median speed was analyzed. It was found that a ±25% speed modulation in one HVAD device at implant resulted in a 26% increase in mean power usage and a 74% increase in peak power usage compared to CF operation at implantation. An average speed modulation of ±20% resulted in an average 6.1% increase in mean power usage ($p = 0.535$)

49

and an average 56% increase in peak power usage ($p = 0.026$) for the VADx devices. Example power and speed waveforms for CF and PF modes for both devices are presented in Figure 11.
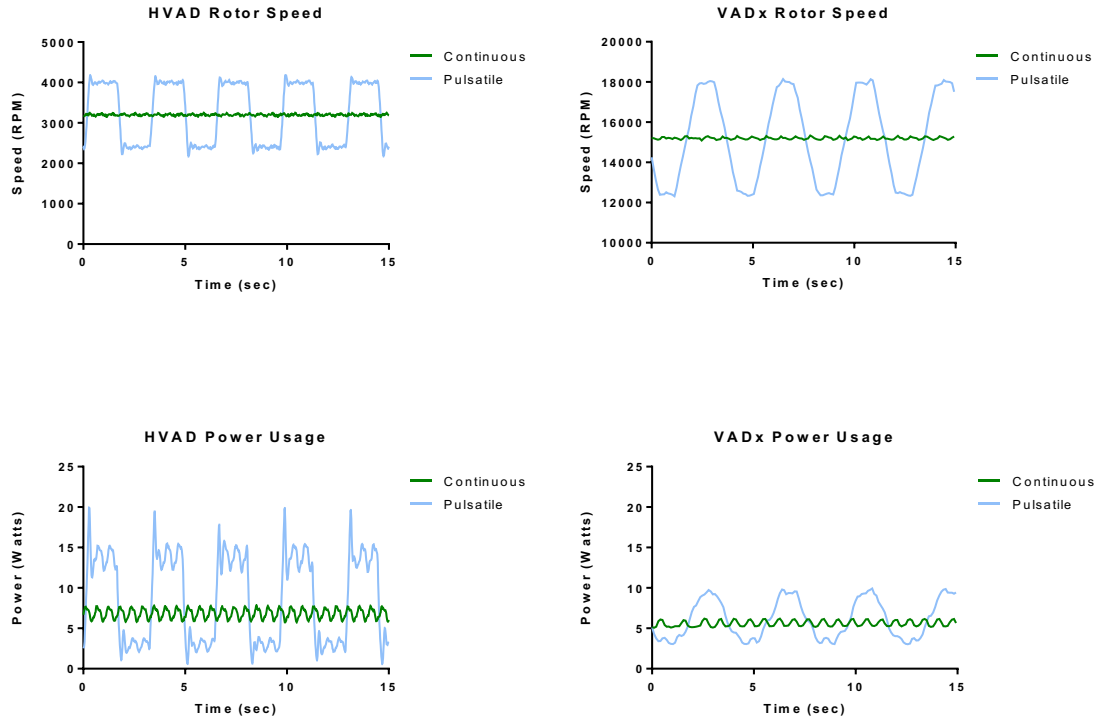
FIGURE 11: Power usage and speed modulation waveforms. Pulsatile modulation increases and decreases rotor speed for set periods of time. In these examples, rotor speed is held at high or low speed for 1.5 seconds before alternating. This pulsatile speed modulation results in a pulsatile power usage as the device uses more power during its highspeed periods. VADx devices sample data less frequently than HVAD devices, explaining the more jagged nature of the waveforms. Rotor speed axes differ and represent the normal operating speed of the respective devices.

C. Left Ventricular Volume Unloading Results

Left ventricular (LV) volume unloading was examined through echocardiographic data taken during the implantation and terminal procedures including SV, EF, and LVEDV. A reduction in SV can indicate an increase in ventricular volume unloading as less volume

is pumped by the heart due to the VAD output. However, the SV can be affected by variation in the HR, therefore the recordings which had the least variation in HR were used for comparison. The HVAD devices reduced SV by an average of 23% from continuous to pulsatile operation during the implantation procedure ($p = 0.333$; 2.5% difference in HR with $p = 0.667$). This shows that asynchronous modulation of the HVAD results in increased volume unloading compared to CF mode (current clinical setting), although the reduction was not statistically significant. The VADx devices reduced SV by an average 27% from the preimplant baseline measurement compared to the pulsatile operational measurement recorded during the terminal procedure ($p = 0.25$; 2.6% difference in HR with $p = 0.875$). Cardiac output followed the same trends as SV but was more affected by the variation in HR.

Typically, in heart failure patients treated with a VAD, LVEDV would decrease as the VAD removes blood from the ventricle and decreases preload indicating volume unloading. However, as seen in Figure 9, LVEDV increased with VADx pulsatile operation during the terminal procedure compared to baseline (22% increase; $p = 0.625$) but decreased in HVAD use (22% decrease; $p = 0.333$). LVEDV did decrease during pulsatile operation compared to CF mode for both devices, indicating that asynchronous modulation possibly results in an increased volume unloading compared to CF. In addition, EF would be expected to increase in heart failure patients with a VAD as the efficiency of the heart increases as the pump reduces the workload. However, EF decreased with VAD usage for both devices as seen in Figure 12. Since the animals used in this study were healthy and not induced into heart failure, the increase in LVEDV for VADx animals and the decrease in EF for both devices would be expected since the device could potentially cause adverse

effects as the heart competes for volume. Preload recruitable stroke work (PRSW) is a linear index of myocardial contractility. Our study found that PRSW increased with device operation. In HVAD devices, PRSW was increased during PF mode compared to CF mode at implantation. In VADx devices, PRSW was higher during CF operation compared to PF mode at the terminal procedure.
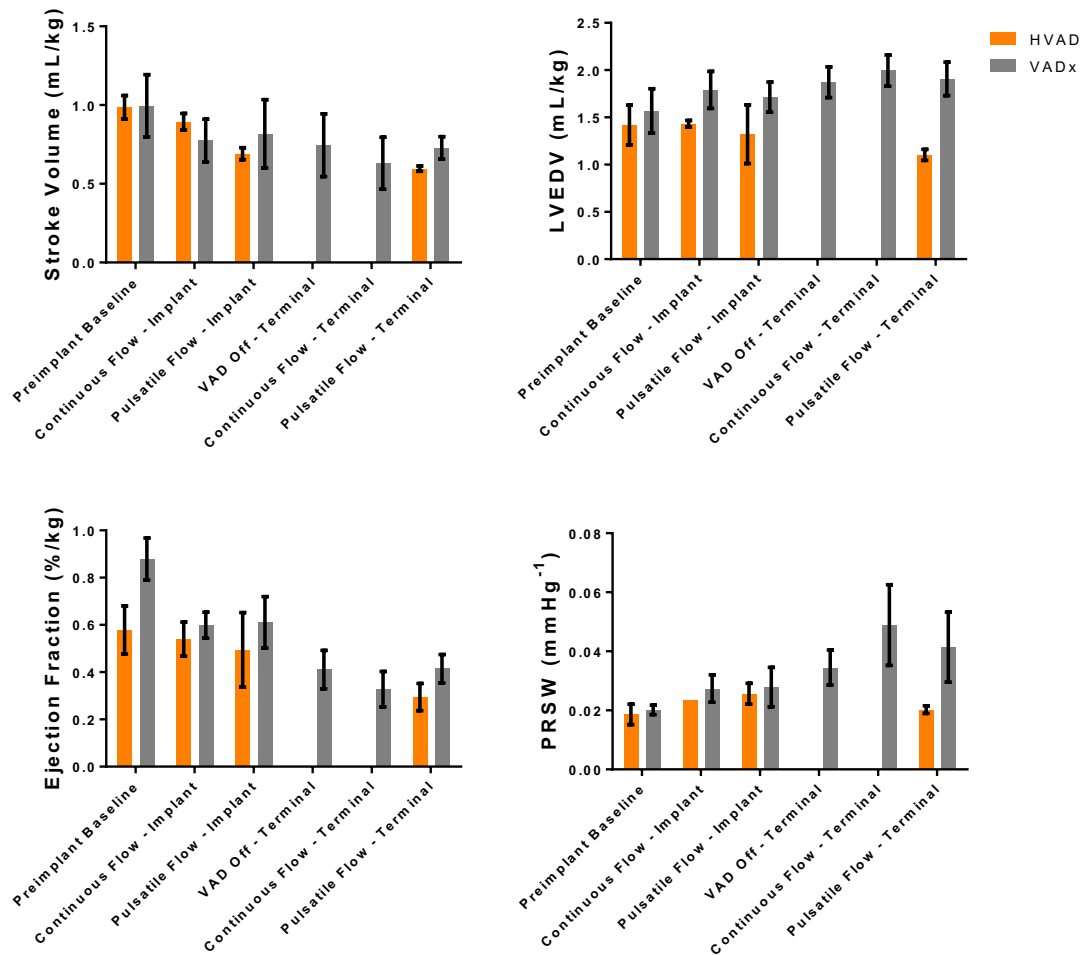
FIGURE 12: Stroke volume (SV), left ventricular end-diastolic volume (LVEDV), ejection fraction (EF), and preload recruitable stroke work (PRSW) for VADx and HVAD devices. SV was reduced from baseline by both devices and no significant difference was found for either device in any test condition ($p > 0.285$). HVAD devices reduced LVEDV from baseline by 22%

while VADx devices increased LVEDV by 22%. EF was reduced with VAD usage for all animals. PRSW increased with device operation but was only increased in PF mode compared to CF mode in HVAD devices; no significant differences were found between operating conditions. These results were normalized to animal weight in order to remove growth as a factor for any potential differences. Preimplant baseline data was collected during implantation procedure before device was inserted into the chest. Data is presented as the mean +/- SEM.

<div align="center">D. Aortic Pulsatility</div>

1. Aortic Pressure Results

Aortic pulsatility was quantified by analyzing changes in hemodynamic pressures and flows between the implantation and terminal procedures. AoP was measured for both HVAD and VADx animals. The pulse pressure is a measure of the pulsatility of the blood flow and pressure waveform through the aorta. During HF, ΔP is diminished as the heart can no longer efficiently contract and exert as great a force on the blood. With a CF-VAD implanted, ΔP is diminished even further. In this study, it was found that ΔP decreased by 6.4% (p = ns) in HVAD animals from directly before device implant (52 ± 13 mmHg) to pulsatile operation during the terminal procedure (48 ± 7 mmHg). ΔP decreased by 20% (p = 0.125) in VADx animals during the same timeframe (49 ± 4 mmHg to 40 ± 2 mmHg). However, the ΔP observed during PF operation during the terminal procedure was still greater than during CF operation for both HVAD and VADx devices as seen in Figure 13. Mean AoP increased from implant to terminal for HVAD animals and decreased for VADx animals, but no significant difference was found between testing conditions.
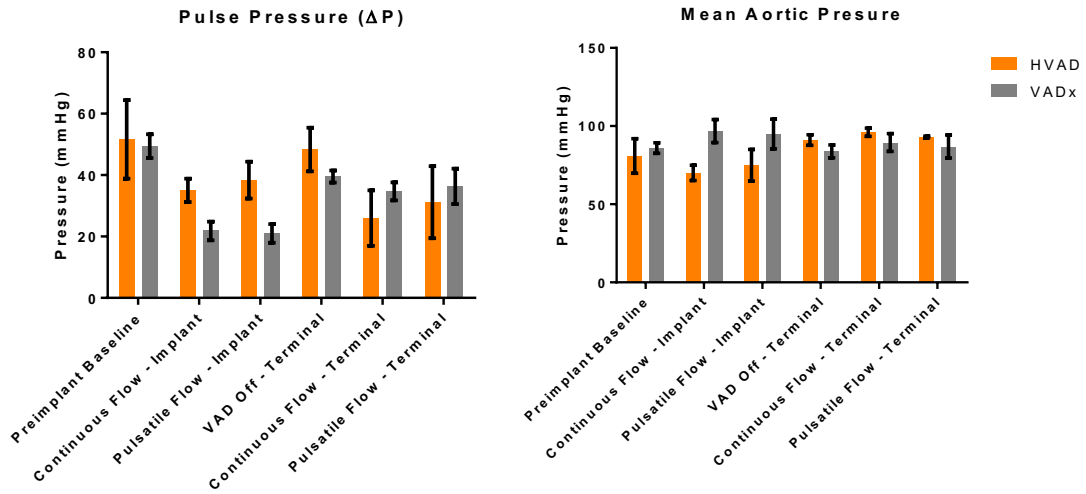
FIGURE 13: Mean aortic pressure and pulse pressure for HVAD and VADx animals. Pulse pressure decreased from baseline values for both devices during operation but was greater in PF mode compared to CF mode. Mean AoP increased in HVAD animals and decreased in VADx animals from baseline values. Preimplant baseline data was collected during implantation procedure before device was inserted into the chest. Data is presented as the mean +/- SEM.

When analyzing the pulse pressure, the overall mean may not take into account the asynchronous, pulsatile expansion of the AoP waveform. Examples of this phenomenon for both devices can be seen in Figure 14. Both waveforms were captured during the post-operative care period during pulsatile modulation. When analyzing the waveform at the largest drop (circled in black), the more accurate pulse pressure induced by the pulsatile modulation can be calculated. Pulsatile operation during these periods for HVAD animals resulted in a pulse pressure of 45 ± 4 mmHg and a pulse pressure of 46 ± 9 mmHg for VADx animals.
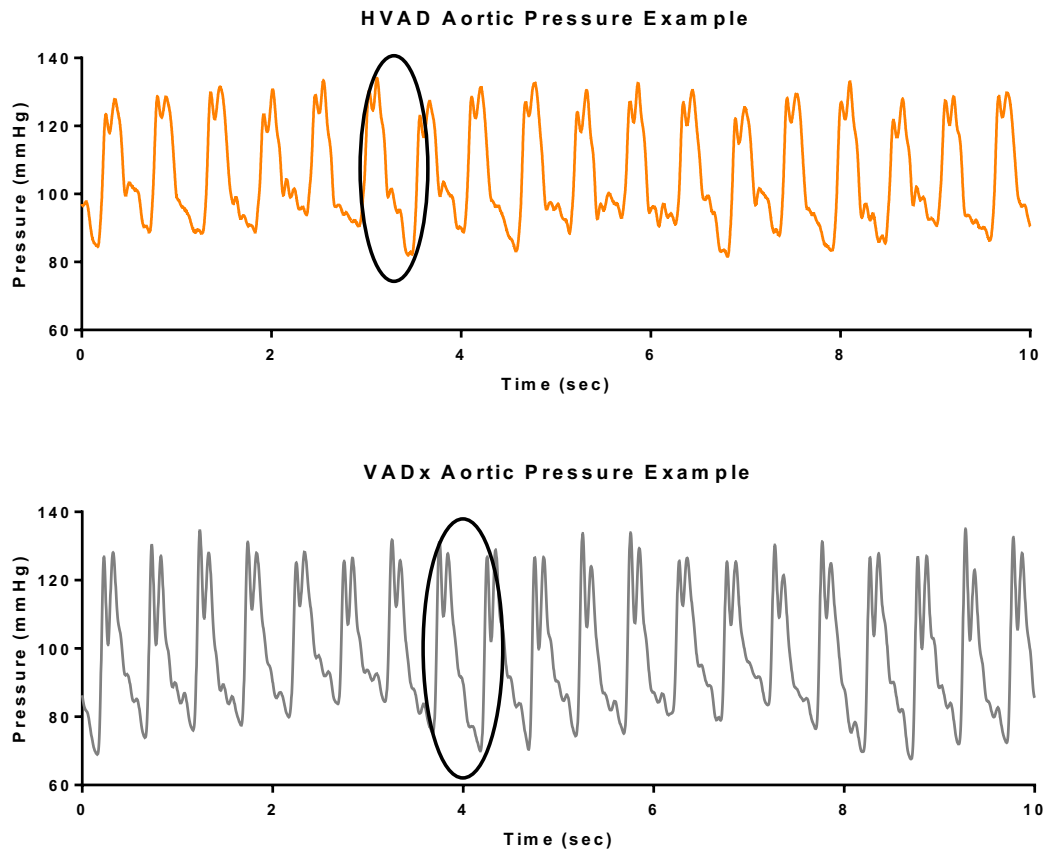
FIGURE 14: Aortic pressure waveform expansion due to pulsatile pump operation.
Sinusoidal, asynchronous effects from pulsatile modulation can be seen in these waveforms.
Analysis of pulse pressure at the end of one pump cycle can give greater insight into the greater
pulse pressure that is induced by asynchronous modulation compared to CF or to co-pulse or
counter-pulsation mechanisms.

The rate of change of the aortic waveform (AoP dP/dt) is another measure to give
insight into the pulsatility of the blood flow. A higher rate of change indicates greater
energy potential and force that the blood has. In Figure 15, it can be seen that both devices
had higher ±dP/dt during PF mode compared to CF. VADx devices had higher ±dP/dt at
the terminal procedure in PF mode compared to baseline.
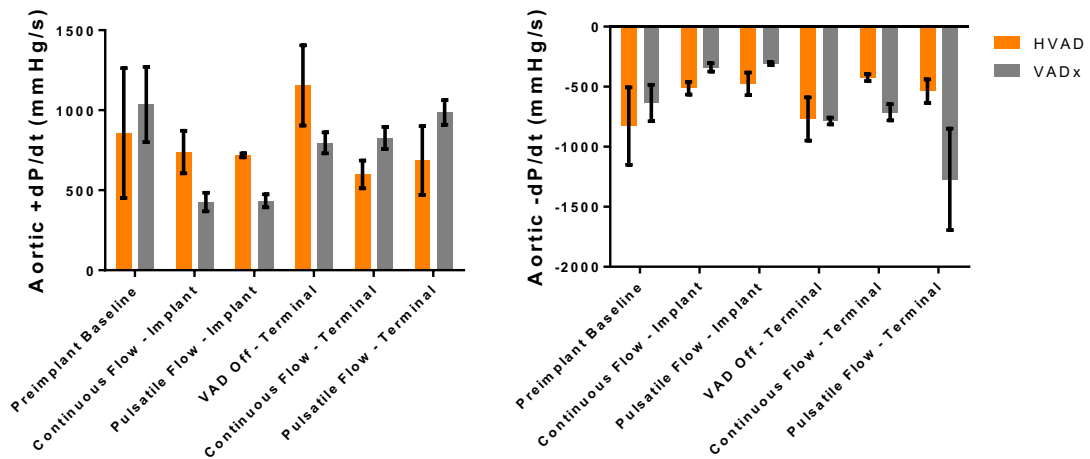
FIGURE 15: Aortic dP/dt for HVAD and VADx animals. HVADs and VADx devices that were asynchronously modulated in PF mode resulted in larger ±dP/dt compared to CF mode. VADx devices had higher ±dP/dt at the terminal procedure in PF mode compared to baseline.

2. HVAD-Specific Results

Additional hemodynamic parameters were able to be analyzed for the HVAD animals to augment pulse pressure data in contrast to VADx animals. Aortic flow was measured before the pump's outflow graft anastomosis to the aorta. The difference between the peak minimum and peak maximum flow (ΔQ) can provide greater insight into the pulsatility of the actual blood flow. As seen in Figure 16, ΔQ decreased during CF mode in HVAD animals as expected and was greater in pulsatile modulation indicating that asynchronous modulation did enhance the actual pulsatility of the blood.

Aortic pressure and flow was measured in the HVAD animals only, enabling calculation of the surplus hemodynamic energy (SHE) and the vascular impedance (ZART). The magnitude of ZART expressed in these results indicates the vascular resistance component of the impedance at the 0th harmonic. The results demonstrated that while SHE decreased from baseline during pump operation, it was greater during PF

compared to CF mode, however no significant difference was found between test conditions ($p = 0.21$). Arterial resistance increased during PF mode compared to CF mode by 4.8% at implantation and 5.1% at the terminal procedure.
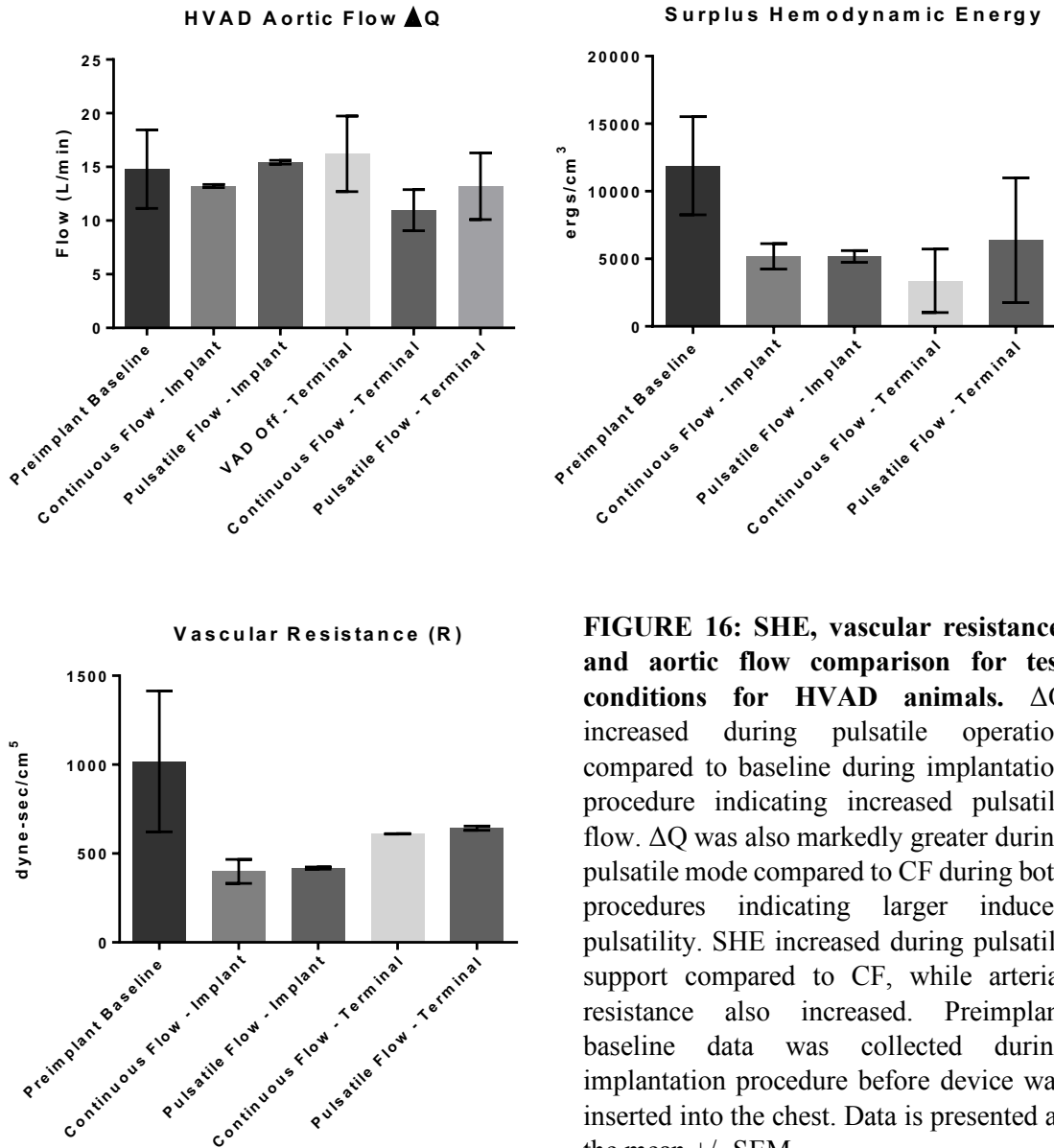
FIGURE 16: SHE, vascular resistance, and aortic flow comparison for test conditions for HVAD animals. ΔQ increased during pulsatile operation compared to baseline during implantation procedure indicating increased pulsatile flow. ΔQ was also markedly greater during pulsatile mode compared to CF during both procedures indicating larger induced pulsatility. SHE increased during pulsatile support compared to CF, while arterial resistance also increased. Preimplant baseline data was collected during implantation procedure before device was inserted into the chest. Data is presented as the mean +/- SEM.

3. <u>VADx-Specific Results</u>

Asynchronous pulsatile modulation resulted in an increased maximum (+) and minimum (-) LV dP/dt at the terminal procedure from baseline by 16% ($p = 0.375$) and 75% ($p = 0.125$) respectively as seen in Figure 17.
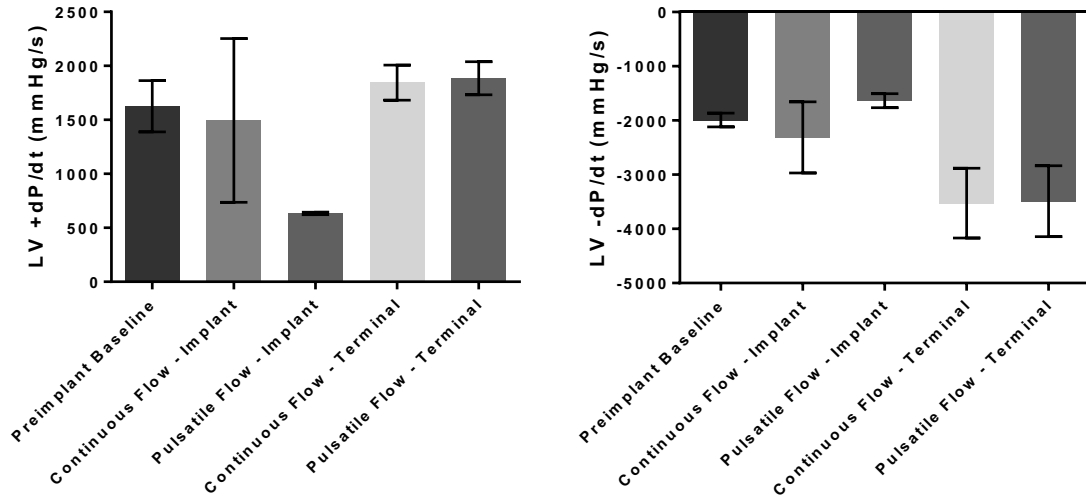
FIGURE 17: Left ventricular pressure (LVP) maximum (+dP/dt) and minimum (-dP/dt) rate of change for VADx animals. Pulsatile operation resulted in increased maximum and minimum rate of change of LVP possibly indicating increased contractility with asynchronous pulsatile modulation. No significant differences between testing conditions was observed for either parameter ($p > 0.088$). Preimplant baseline data was collected during implantation procedure before device was inserted into the chest. Data is presented as the mean +/- SEM.

E. <u>Post-Operative Hematologic Data</u>

Blood samples were collected periodically throughout the post-operative care period to assess animal health and/or the effect of the device on animal health. For all figures in this section, each data point represents the average for all animals' blood collections on that day. Only arterial blood samples were statistically analyzed to eliminate error in oximetry and chemistry results. Horizontal errors bars represent the variation in days that

arterial blood was drawn near the study end for VADx animals. Vertical error bars represent the standard error of the mean for the data. Dashed lines represent normal limits for bovine animals obtained from *Laboratory Animal Medicine* (Underwood et al., 2015). Baseline data was recorded prior to the day of implant, and post-operative day zero represents data collected in the post-operative care room after surgery on the day of implant.

Complete blood count data was measured to assess overall animal health during the post-operative care period. White blood cell (WBC) count was initially elevated during the first two days post-implantation as expected due to the surgical stress experienced by the animals and then fell to within normal limits for the duration of care. Lymphocytes (LY) decreased initially post-implant but returned to normal limits shortly thereafter. Neutrophils (NE), red blood cell (RBC) count, platelet count, and hematocrit remained within normal limits for the duration of care. Trendline graphs for WBC, LY, NE, RBC and platelet count, and hematocrit can be seen in Figure 18.
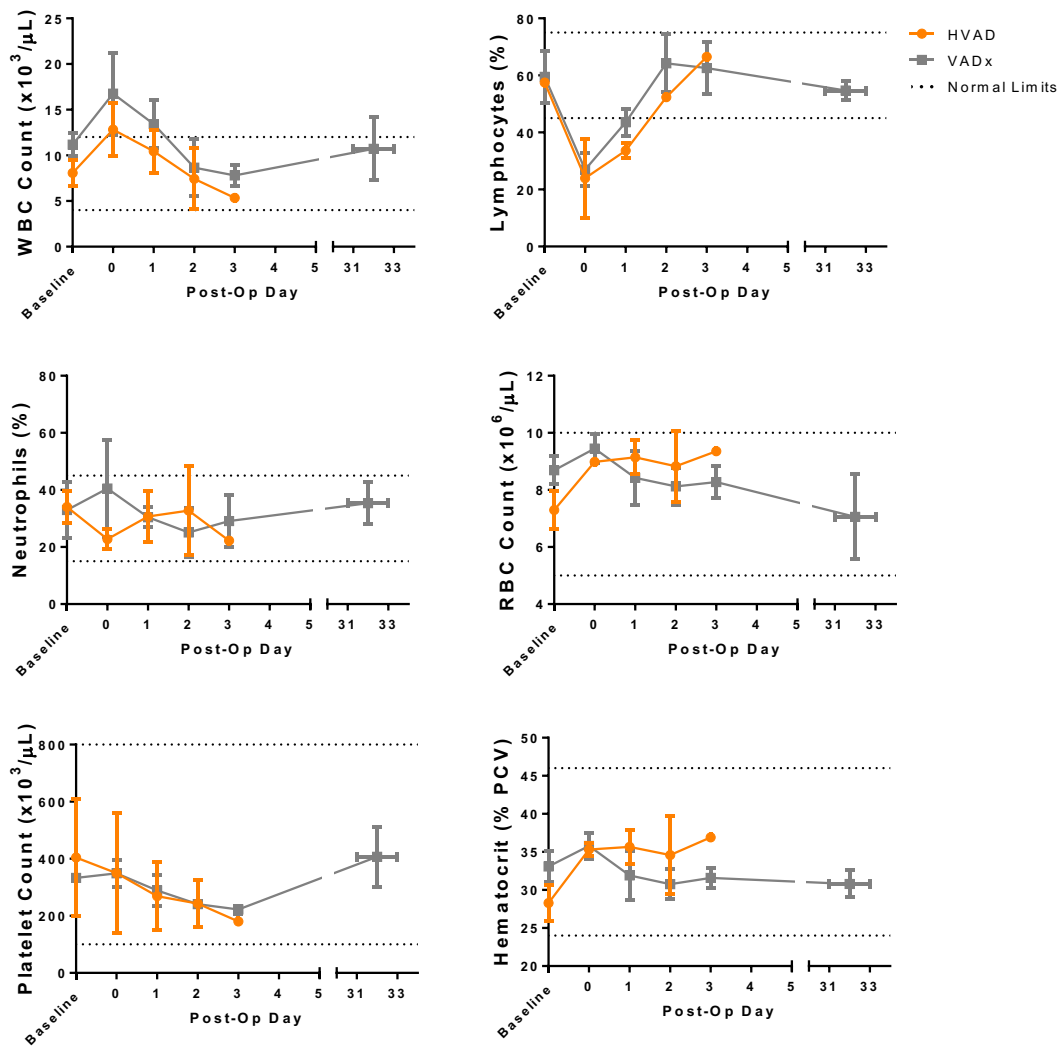
FIGURE 18: Post-operative hematologic biochemistry trends for HVAD and VADx animals.
WBC was initially elevated post-implant as expected due to the surgical stress experienced by the animals and then remained within normal limits for the duration of the study. LY were initially decrease post-implant but shortly returned to within normal limits. NE, RBC, platelet count, and Hct remained within normal limits throughout the study duration.

Prothrombin time (PT)/international normalization ratio (INR) and activated clotting time (ACT) testing was done to ensure that anticoagulation was kept to adequate levels to prevent pump thrombosis. ACT was kept within the targeted range of 200-300 seconds for

both HVAD and VADx animals. INR was initially below the normal range on post-operative days 1 and 2 and then stayed within the normal range for HVAD animals through the duration of care. For VADx animals, INR was within normal limits except for days 18-26 when it became elevated with an average of 3.8 and 4.6 measured on days 18-22 and 23-27 respectively. Trendline graphs for these measurements can be seen in Figure 19.
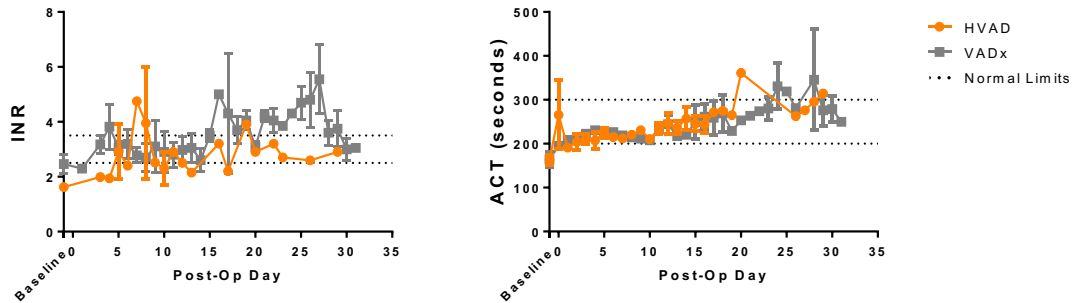
FIGURE 19: Post-operative trends for blood coagulation data. Animals were treated with heparin and coumadin during the post-operative care period to target an ACT of 200-300 which was maintained throughout the study duration. INR remained within normal limits with the exception of VADx animals around post-operative day 25 due to one animal as explained in the pfHb section.

Blood chemistry and oximetry data was collected to assess end-organ perfusion, nutrient transfer, and tissue damage. Serum sodium (Na^+), potassium (K^+), and ionized calcium (Ca^{2+}) were within normal limits for the duration of post-operative care for both HVAD and VADx animals. Serum chloride (Cl^-) was slightly below the normal range, however the 30-day post-operative averages for HVAD and VADx animals were within their baseline values. Therefore, blood chemistry did not appear to be affected by pulsatile modulation of the VADs. Blood glucose levels were elevated from the normal range, and the 30-day averages were 3% and 35% greater than baseline values for HVAD and VADx

animals respectively. Normal oxygen saturation was maintained by all animals throughout the study duration. pH, pCO2, and bicarbonate (HCO_3^-) remained within normal limits for both devices with the exception of VADx animals near the study end point. pO2 was near normal limits except for post-operative day zero for both devices as the animals were on 100% oxygen following the implantation. One VADx animal was observed to have greatly elevated pO2 near the study end-point. Lactate dehydrogenase (LDH) was elevated from baseline values in the initial days following implantation as expected. However, LDH levels did not begin to fall and return to baseline values until around post-operative day 20. The 30-day LDH average was only 56% greater than baseline in VADx animals and 124% greater than baseline HVAD animals. The trends for all analyzed blood chemistry and oximetry data can be seen in Figures 20 and 21.
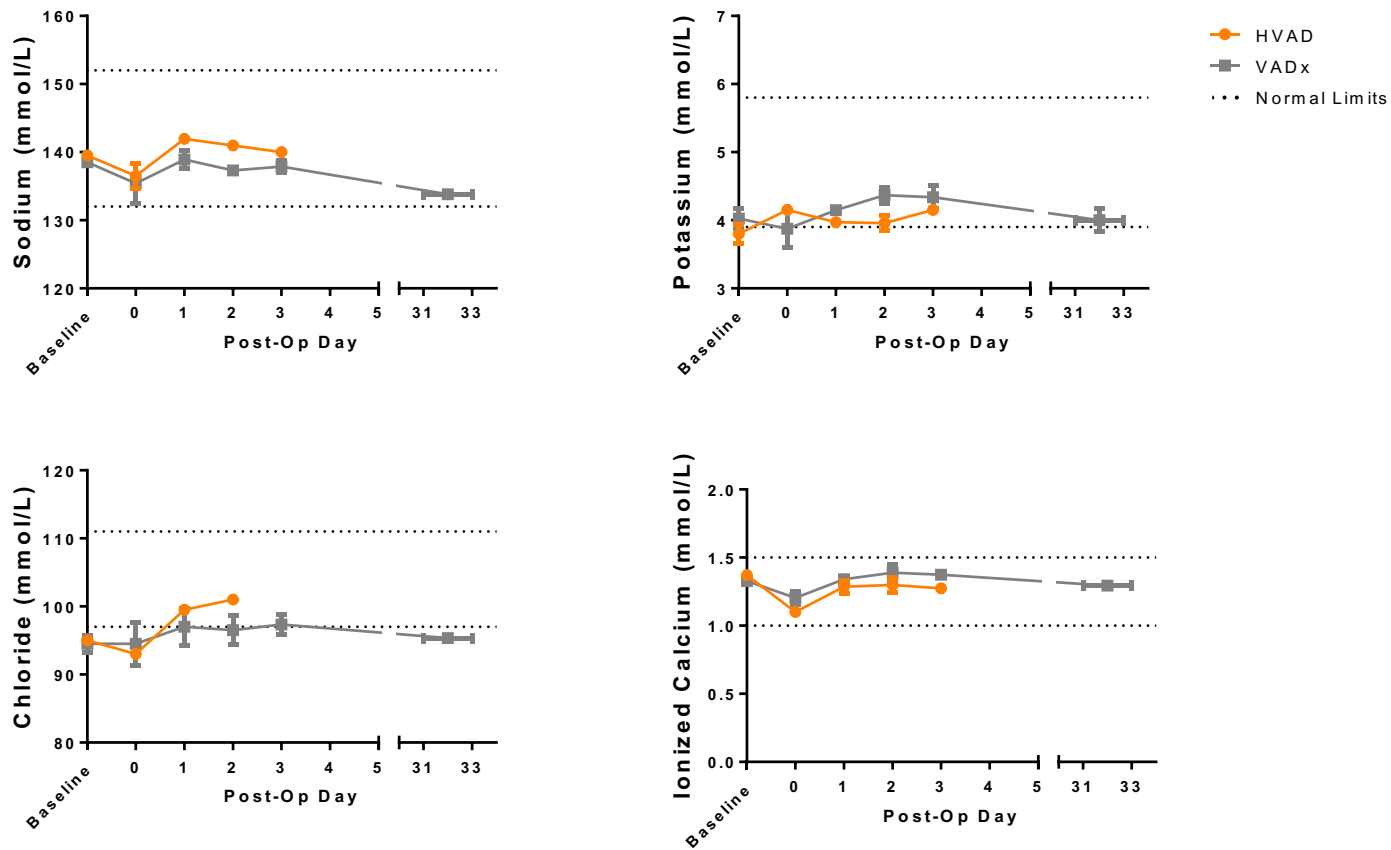
FIGURE 20: Blood chemistry and oximetry trends for the post-operative care period. Serum Na^+, K^+, and Ca^{2+} were within normal limits for the duration of post-operative care. Cl^- was slightly below the normal range, but post-operative averages for both devices were within 4% of baseline values.
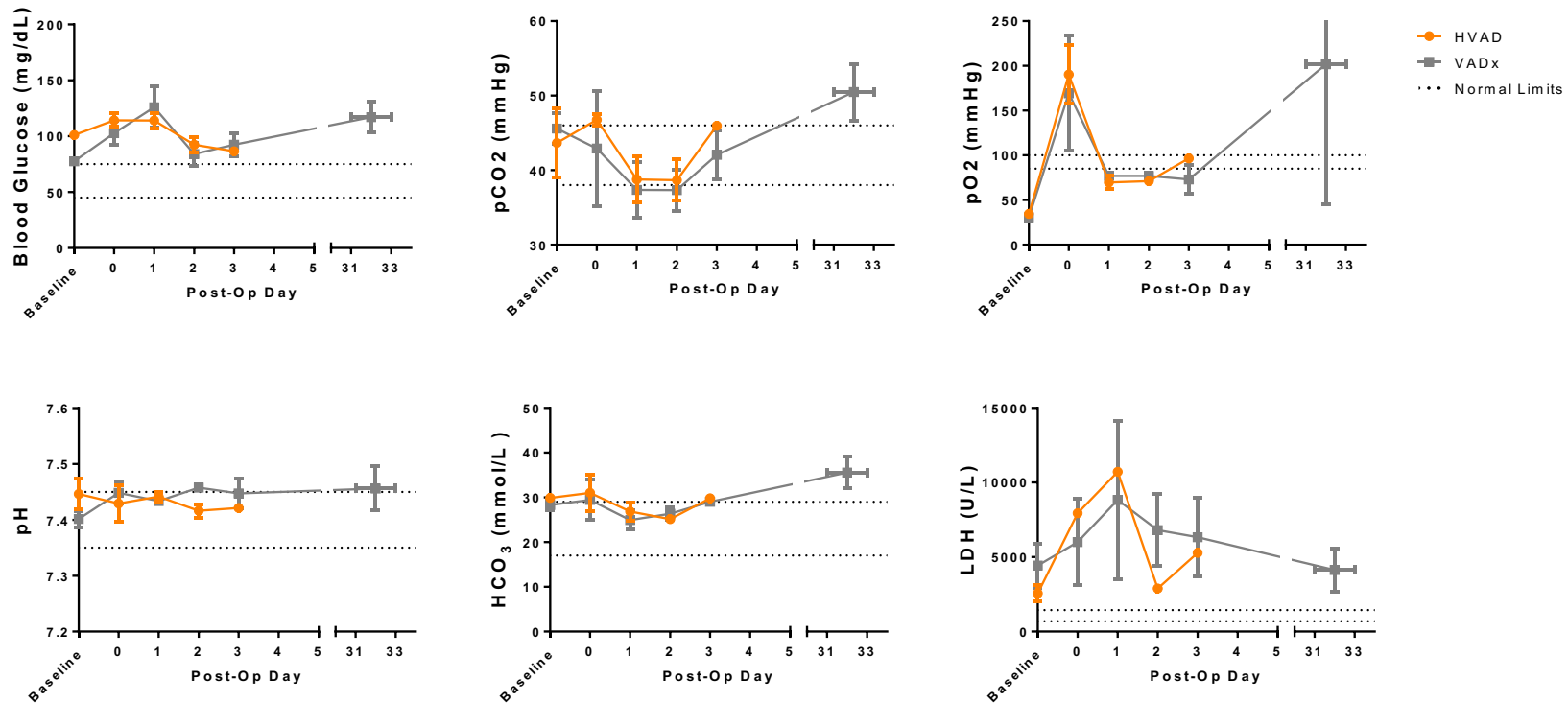
FIGURE 21: Blood chemistry and oximetry trends for the post-operative care period (continued). LDH was elevated initially post-implantation as expected but did not return to baseline levels until post-operative day 20. HCO_3^-, pH, pO2, and pCO2 remained near normal limits during the study duration.

Plasma-free hemoglobin (pfHb) was measured throughout the post-operative care period to monitor for and assess any signs of hemolysis or thrombosis. Animals implanted with an HVAD device did not have pfHb exceeding 10 mg/dL throughout the study duration. VADx pfHb results were elevated during post-operative days 15-26 after which pfHb returned to baseline levels. This elevated pfHb can be attributed to one animal, assigned animal #5914, whom experienced a spike in pfHb at post-operative day 16 which remained elevated until post-operative day 25. The post-operative trend for this animal's pfHb results and the average pfHb for both devices can be seen in Figure 22.
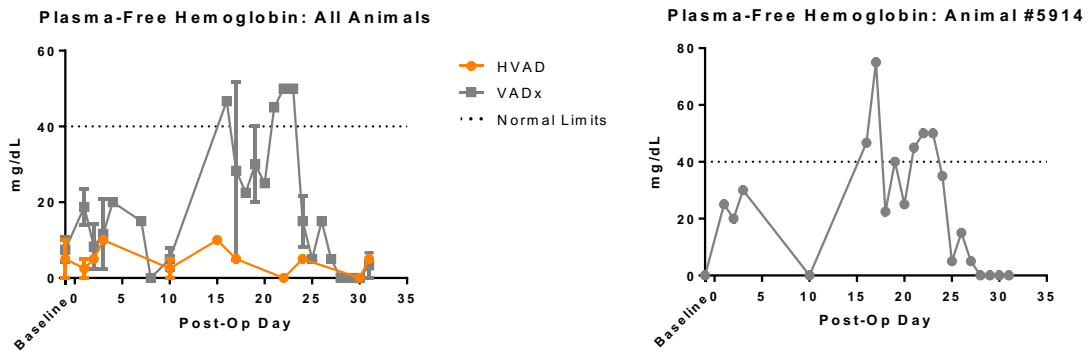
FIGURE 22: Post-operative trends for plasma-free hemoglobin (pfHb) and individual 30-day results for animal #5914. pfHb was within normal limits (0 to 40 mg/dL) for both devices throughout the post-operative care period. However, VADx devices experienced elevated pfHb around post-operative days 15-25 due to animal #5914 which appeared to have experienced a thrombotic event resulting in a spiked pfHb.

While investigating the pfHb spike, it was found that animal #5914 had an associated spike in device power usage. The device was subsequently turned to CF mode on post-operative day 18, then turned back to pulsatile modulation the next day. The operating speed for the device was lowered when modulation resumed, then lowered again on post-operative day 25. Plasma-free hemoglobin results for this animal improved to baseline

levels on day 25 and never became elevated afterwards. This data suggests that animal #5914 had experienced a thrombotic episode during this period which later subsided. In the same vein as pfHb, the elevated LDH levels in VADx animals can be partially attributed to animal #5914 whose measured LDH was 185% greater than the average of the remaining VADx animals on post-operative day 24. Like pfHb, LDH for animal #5914 eventually returned to baseline levels after the device's operating mode and speed was modified. Normal ranges, baseline values, and post-operative averages for all analyzed hematologic data are reported in Tables II-VI.

The presence of valve regurgitation during the implantation and terminal procedures was determined through echocardiographic data analysis. No mitral insufficiency was found, and only nominal aortic insufficiency was found during implantation for one HVAD animal and one VADx animal and during the terminal procedure for one VADx animal.

TABLE III

NORMAL RANGES, BASELINE VALUES, AND POST-OPERATIVE AVERAGES FOR HEMATOLOGIC DATA

		INR	ACT (seconds)	pfHb (mg/dL)	pH	pCO2** (mmHg)	pO2** (mmHg)	BEecf (mEq/L)	HCO3- (mmol/L)	TCO2 (mmol/L)
Normal Range*		2.5-3.5	200-300	< 40	7.35-7.45	38-46	85-100	(±3)	17-29	21.2-32.2
HVAD	Baseline	1.62 ± 0.04	163 ± 12	5.0 ± 5.0	7.45 ± 0.03	43.7 ± 3.3	34.5 ± 2.5	6.0 ± 0.0	29.9 ± 0.3	31.5 ± 0.5
	PO Average	2.83 ± 0.20	242 ± 7	4.2 ± 1.0	7.43 ± 0.01	42.1 ± 1.7	108.4 ± 22.1	3.5 ± 1.3	28. ± 1.2	29.1 ± 1.2
VADx	Baseline	2.47 ± 0.35	164 ± 18	7.5 ± 3.2	7.40 ± 0.01	45.6 ± 1.0	30.8 ± 1.5	3.5 ± 0.6	28.3 ± 0.5	29.8 ± 0.5
	PO Average	3.42 ± 0.12	242 ± 5	16.6 ± 2.8	7.45 ± 0.01	42.1 ± 1.7	122.7 ± 21.3	4.9 ± 1.3	29. ± 1.2	30.1 ± 1.3

*Normal range for bovine obtained from *Laboratory Animal Medicine* (Underwood et al., 2015)

**Venous blood samples were used for baseline data, explaining the large differences in partial pressures compared to PO averages.

All results expressed as mean ± standard error of the mean. Post-operative (PO) averages are the means for all arterial blood sample data collected post-implantation during the post-operative care period. All blood data results were within normal limits as shown or with minimal deviations from baseline values. BEecf: base excess; TCO_2: Total CO_2.

TABLE IV

NORMAL RANGES, BASELINE VALUES, AND POST-OPERATIVE AVERAGES FOR HEMATOLOGIC DATA (CONTINUED)

		Na+ (mmol/L)	K+ (mmol/L)	Cl- (mmol/L)	Ca2+ (mmol/L)	Glucose (mmol/L)	BUN (mg/dl)	Creatine (U/L)	LDH (U/L)
Normal Range*		132-152	3.9-5.8	97-111	1.0-1.5	45-75	20-30	1-2	692-1445
HVAD	Baseline	140 ± 1	3.80 ± 0.1	95.0 ± 0.0	1.37 ± 0.01	101 ± 1.0	11 ± 1.0	0.45 ± 0.05	2565 ± 395
	PO Average	140 ± 1	4.05 ± 0.0	98.8 ± 1.5	1.24 ± 0.04	104 ± 5.2	11 ± 2.9	0.52 ± 0.10	7510 ± 1533
VADx	Baseline	139 ± 0.3	4.03 ± 0.1	94.5 ± 0.6	1.33 ± 0.01	78 ± 1.2	11 ± 2.6	0.60 ± 0.06	4427 ± 1048
	PO Average	137 ± 0.5	4.14 ± 0.1	96.1 ± 0.6	1.31 ± 0.02	105 ± 4.6	10 ± 0.7	0.47 ± 0.03	6296 ± 805

*Normal range for bovine obtained from *Laboratory Animal Medicine* (Underwood et al., 2015)

All results expressed as mean ± standard error of the mean. Post-operative (PO) averages are the means for all arterial blood sample data collected post-implantation during the post-operative care period. With the exception of LDH and blood glucose, all blood data results were within normal limits as shown or with minimal deviations from baseline values. BUN: blood urea nitrogen.

TABLE V

NORMAL RANGES, BASELINE VALUES, AND POST-OPERATIVE AVERAGES FOR HEMATOLOGIC DATA (CONTINUED)

		WBC Count (x10^3/μL)	NE (%)	LY (%)	MO (%)	EO (%)	BA (%)	RBC Count (x10^6/μL)
Normal Range*		4-12	15-45	45-75	2-7	2-20	0-2	5-10
HVAD	Baseline	8.07 ± 1.01	34.1 ± 3.9	57.5 ± 0.9	4.1 ± 0.5	4.3 ± 2.6	0.05 ± 0.05	7.30 ± 0.47
	PO Average	9.53 ± 1.33	27.8 ± 3.4	40.9 ± 6.5	4.8 ± 1.1	26.4 ± 7.9	0.09 ± 0.04	9.04 ± 0.23
VADx	Baseline	11.17 ± 0.64	32.9 ± 4.8	59.5 ± 4.6	5.6 ± 1.0	1.9 ± 0.6	0.08 ± 0.04	8.69 ± 0.24
	PO Average	11.72 ± 1.05	32.1 ± 2.5	49.5 ± 3.7	5.0 ± 0.6	13.4 ± 3.6	0.12 ± 0.02	8.33 ± 0.25

*Normal range for bovine obtained from *Laboratory Animal Medicine* (Underwood et al., 2015)
All results expressed as mean ± standard error of the mean. Post-operative (PO) averages are the means for all arterial blood sample data collected post-implantation during the post-operative care period. All blood data results were within normal limits as shown or with minimal deviations from baseline values.
WBC: white blood cell; NE: neutrophils; LY: Lymphocytes; MO: monocytes; EO: eosinophils; BA: basophils; RBC: red blood cells.

TABLE VI

NORMAL RANGES, BASELINE VALUES, AND POST-OPERATIVE AVERAGES FOR HEMATOLOGIC DATA (CONTINUED)

		Hemoglobin (g/dL)	Hematocrit (% PCV)	MCV (fl)	MCH (pg)	MCHC (g/dL)	Platelet Count (x10^3/μL)	MPV (fl)
Normal Range*		8-15	24-46	40-60	11-17	30-36	100-800	4.5-7.5
HVAD	Baseline	8.55 ± 0.05	28.3 ± 1.7	38.9 ± 0.1	11.8 ± 0.8	30.3 ± 2.0	405 ± 146	5.1 ± 0.6
	PO Average	10.83 ± 0.18	35.4 ± 0.9	39.2 ± 0.1	12.0 ± 0.2	30.6 ± 0.5	272 ± 46	4.7 ± 0.2
VADx	Baseline	10.59 ± 0.25	33.1 ± 1.0	38.1 ± 0.7	12.2 ± 0.3	32.0 ± 0.6	333 ± 7	4.5 ± 0.1
	PO Average	10.08 ± 0.26	32.3 ± 0.6	39.1 ± 0.9	12.2 ± 0.2	31.2 ± 0.4	300 ± 19	4.7 ± 0.1

*Normal range for bovine obtained from *Laboratory Animal Medicine* (Underwood et al., 2015)
All results expressed as mean ± standard error of the mean. Post-operative (PO) averages are the means for all arterial blood sample data collected post-implantation during the post-operative care period. All blood data results were within normal limits as shown or with minimal deviations from baseline values.
MCV: mean corpuscular volume; MCH: mean corpuscular hemoglobin; MCHC: mean corpuscular hemoglobin concentration; MPV: mean platelet volume.

IV. <u>DISCUSSION</u>

A. <u>Overview/Key Findings</u>

We have previously reported the feasibility of asynchronous modulation of CF-VADs to generate pulsatility and ventricular volume unloading in mock circulatory loop and heart failure bovine models for acute durations (Ising et al., 2015; Soucy et al., 2015). To investigate long-term effects of asynchronous modulation and build on our previous findings, a 30-day chronic, healthy bovine model was used in this study. In addition, echocardiographic data was used to calculate LV volumes and examine ventricular volume unloading in contrast to pressure-volume catheters placed directly into the ventricle which are frequently used. Pump speed modulation in the VADx device has never previously been implemented, and this study showed its feasibility and chronic effects.

The use of healthy animals in this study created a partial VAD support model that showed chronic asynchronous pulsatile modulation of CF-VADs maintained aortic pulsatility and reduced stroke volume. LVEDV was reduced in HVAD animals but slightly increased in VADx animals. While EF was reduced in all animals, this could have been due to limitations in the study design. Minimal increase in power usage and hemolysis occurred potentially indicating that asynchronous modulation can be practically implemented into current CF-VADs for long-term support.

69

B. <u>Pulsatility</u>

Several studies have modulated CF-VAD speeds to examine the effects on aortic pulsatility. Bozkurt et al. utilized a mock circulatory loop with an ex-vivo porcine heart controlled by a pacemaker to test their novel proportional-integral (PI) controller for device outflow in a MicroMed DeBakey VAD (Bozkurt et al., 2014). The PI controller set the pump flow rate, the control variable, during the first $1/4^{th}$ of the cardiac cycle. Pump flow rate was measured via a Transonic flow probe located in the pump outflow graft, a feature of the DeBakey VAD. They found that this co-pulse synchronized algorithm doubled the pulse pressure, pulsatility index, and amplitude of VAD flow in the aorta. Arakawa et al. tested their previously developed co-pulse synchronized algorithm for the EVAHEART VAD at fixed heart rates in healthy goats and at native heart rates in chronic heart failure goats (Arakawa et al., 2016). Their algorithm monitored the ECG and increased pump speed for a set amount of time when an R wave was detected. Pulsatile mode produced greater pulse pressure and AoP maximum dP/dt than continuous mode and resulted in a higher EEP at lower heart rates. While these studies used different pumps and implemented co-pulse synchronized algorithms differently, the results are consistent and support the findings in our study by showing asynchronous modulation is able to increase pulsatility because of intermittent periods of co-pulsation.

In a clinical setting, Travis et al. investigated differences in aortic pulsatility between CF-VADs and PF-VADs (Travis et al., 2007). Hemodynamic pressure and flow waveforms were collected intraoperatively in patients with normal ventricular function (undergoing coronary artery bypass) and heart failure patients implanted with either a PF-VAD (Thoratec HeartMate XVE or Thoratec IVAD) or CF-VAD (Thoratec HeartMate II or

MicroMed DeBakey VAD). In the PF-VAD group, SHE values were restored to baseline levels at low VAD speed and augmented at high VAD speed, while SHE was reduced with increasing support in the CF-VAD group. Travis et al.'s findings support the results of our study that found increased SHE during PF modulation of HVADs compared to CF mode, demonstrating this model's relevance to predicting potential clinical observations.

<p style="text-align:center">C. <u>Volume Unloading</u></p>

A study examining pulsatility and volume unloading in a healthy goat model with a speed-modulated EVAHEART VAD by Date et al. found that LV load increased significantly during co-pulse modulation compared to counter-pulse modulation (Date et al., 2016). The findings of Date et al. suggest the possible benefit of asynchronous modulation of CF-VADs in severe heart failure patients. Asynchronous modulation would provide intermittent periods of LV loading and unloading which would provide simultaneous rest and stimulation for a failing ventricle. This characteristic of asynchronous modulation could possibly explain the inconsistent LVEDV effects observed between the devices in our study but supports that volume unloading was augmented as evidenced by our observed decrease in SV.

Kato et al. investigated volume unloading in heart failure patients implanted with either a PF-VAD (HeartMate XVE or Thoratec PVAD) or CF-VAD (HeartMate II, Duraheart, or DeBakey VAD) and found that pulsatile devices improved LV systolic and diastolic function (Kato et al., 2011). In particular, it was found that PF-VADs significantly increased EF, while CF-VAD patients did not experience an increased EF. These findings do not match the results in this study which observed that EF decreased in all animals during the study duration, however it was observed that EF was increased in pulsatile mode

in VADx animals. This discrepancy may be attributed to study limitations, most notably that healthy animals likely have different cardiac physiology and responses to VAD support than the heart failure patients who participated in Kato et al. Our study also found that LV +dP/dt was higher in PF mode than CF mode in VADx animals which is consistent with Kato et al.'s observation that PF-VADs resulted in greater improvement in and larger +dP/dt compared to CF-VADs. This indicates that pulsatile modulation and PF-VADs may potentially increase LV contractility leading to greater LV unloading.

D. Blood Trauma and Power Consumption

Additional consideration should be given to the increased power requirements and potential blood trauma that could result from CF-VAD speed modulation. While our study examined blood trauma via pfHb, other methods of detecting blood trauma such as platelet activation and von Willebrand factor (vWf) can provide additional insights into the true effects of high shear stress on the blood, however these methods are not routinely used in clinical settings (Pirbodaghi, Asgari, et al., 2014). It is possible that pulsatile modulation algorithms can affect the hemocompatibility of the device due to different shear stress profiles. A recent study by Horobin et al. found that there was no difference in hemocompatibility biomarkers such as platelet aggregation and concentrations of vWf, ADAMTS13, and pfHb in plasma when comparing pulsatile and continuous flow with an HVAD device in a mock circulatory loop utilizing human donor blood (Horobin et al., 2018). Our study found that five of the six animals with devices operated in asynchronous modulation maintained pfHb within clinical range for CF-VAD devices. While our results indicate the other animal possibly experienced a brief thrombotic event which was resolved, the cause for the event remains unidentified. Our findings and those of Horobin

et al. may indicate that chronic pulsatile modulation of CF-VADs does not further adversely affect hemocompatibility and hemolysis compared to current clinical practice of fixed mean speed CF-VAD use.

Our study found that mean device power consumption increased during asynchronous modulation compared to CF in HVADs by 26% at implant and 8.7% at the terminal procedure and in VADx devices by 6.1% at implant and 9.5% at the terminal procedure, and the increase was similar to that found by Soucy et al. which used HVADs in a heart failure bovine model (Soucy et al., 2015). Pirbodaghi et al. examined power consumption for the HeartMate III (Abbott) in a mock circulatory loop and found that pulsatile mode resulted in less than a 2.5% increase in power consumption for any given rotor speed (Pirbodaghi, Cotter, et al., 2014). Although the increase in power consumption with a HeartMate III was substantially less than that observed in our study or in Soucy et al., the pressure gradient in Pirbodaghi et al. was also substantially lower (0 mmHg) than our study (about 100 mmHg). These findings suggest that pulsatile modulation may result in increased power usage but may not have a major clinical impact on outcomes or power supply requirements.

E. Engineering Considerations

Since the animals used in this study were healthy and not induced into heart failure, the native cardiac output exceeded device output limits. This created a model that could inherently provide only partial VAD support. Full VAD support of the LV was shown to be correlated with aortic valve stasis and myocardial atrophy (A. H. Goldstein et al., 2005). In response, partial VAD support was proposed to counter these issues since partial unloading of the LV allows for aortic valve opening and animation. Previously, partial

support has been shown to provide beneficial effects on preload and afterload of the LV in a computational fluid dynamics model and an acute bovine experiment (Morley et al., 2007). Partial VAD support was also shown to decrease myocardial oxygen consumption in a chronic heart failure ovine model which can be indicative of myocardial workload reduction (A. H. Goldstein et al., 2005). In a clinical setting comparing full and partial VAD support, partial support was associated with improved myocardial function and blood flow (Maybaum et al., 2002). these results may indicate that partial unloading of the left ventricle can improve ventricular function, the effects on the pulsatility of the blood cannot easily be examined. With a partial support model, the heart is still ejecting with each beat and is contributing to the pulsatility of the blood flow. The influence of modulated CF-VAD flow on the pulsatility cannot easily be measured, therefore the maintenance of near-physiologic aortic pulsatility is can be a better comparison between CF and PF modes. Our study did find that aortic pulse pressure was higher in PF mode compared to CF mode, possibly indicating better maintenance of near-physiologic pulsatility.

However, this introduces a concern in the comparison of CF to PF mode. Our study fixed CF mode at a set pump speed, then set PF mode in order to match its median speed with the speed of CF mode. In a partial support model, the level of cardiac output can differ between animals in this configuration and therefore comparisons between CF and PF mode may be limited. Another configuration for CF and PF mode comparisons can be created by changing each mode's settings to produce the same fixed level of cardiac support. This configuration would give greater meaning to comparisons made between PF and CF mode including power and pulsatility measurements. However, when briefly testing the output of both operational modes in HVAD animals, we observed that setting the median speed

of the PF mode to the fixed CF mode speed resulted in the same level of VAD support in both operational modes. Unfortunately, the VADx devices were unable to be tested in this way during this study due to the lack of flow instrumentation. Further experimentation using a mock circulatory loop and volume output normalized to time could determine if this configuration results in similar VAD support levels with the VADx device.

When testing the devices by fixing the desired support level between operational modes, the effects of further modifying the amplitude and frequency of asynchronous modulation can be examined. Pulsatility of the blood flow can be enhanced by increasing the difference between the high and low speeds. Mean pressure can be adjusted by shifting this window up or down the device's operational speed range. LV unloading can be adjusted during PF mode with the same level of VAD support as CF mode by adjusting the frequency of the asynchronous modulation. Previously, we found that lower frequencies (higher duty cycles) of asynchronous modulation resulted in higher pulse pressure and lower LV external work (Soucy et al., 2015). This effect may be due to the longer periods of partial loading and unloading of the ventricle. However, this also may suggest that synchronized modulation may provide better outcomes in partial support models due to the ability to specifically target LV unloading since the heart can induce native pulsatility through its own contribution to the blood flow.

Finally, the VAD's outflow graft anastomosis to the aorta can affect the flow pattern and pulsatility of the blood. The HVAD outflow graft is anastomosed end-to-side on the descending aorta which can create areas of turbulent blood flow at the junction. Depending on the angle of the anastomosis, blood flow can recirculate around the junction from the VAD's flow and enter back into the outflow graft or travel in either direction (with or

against native blood flow) in the aorta. This turbulence can potentially reduce the pulsatility of the blood flow in the aorta as the VAD flow detracts from native cardiac output. The VADx device does not experience this phenomenon since it's outflow cannula is positioned in line with native cardiac output in the aorta. However, the cannulation of the VADx across the aortic valve has its own concerns. For instance, the repeated opening and closing of the aortic valve around the outflow cannula with partial VAD support may cause bruising of the valve leaflets. Another consideration in our study model was that the cannula size had to be chosen to ensure that the tip did not retract into the LV when the animal grew.

F. Limitations

This study has several potential limitations. First, the calves used in this study were chosen to be small (about 50 kg), however the HVAD animals had a longer period between arrival and implantation compared to the VADx animals explaining their larger starting weight. Second, we used healthy calves as opposed to a clinically relevant heart failure model that would have differences in cardiac output and vascular compliance of the animals. Third, our study design with calves is not conducive for chronic instrumentation with indwelling catheters; therefore, the majority of our data was recorded during the implantation and terminal procedures. Fourth, since implantation of the VADx device only requires a mini thoracotomy, the need for a large cut to insert the device and other instrumentation is negated. Therefore, since we could not acquire blood flow data in these animals, other measures of pulsatility such as SHE and EEP could not be calculated. Fifth, volumetric analysis was limited to the accuracy of the QLAB software in tracking of the ventricular wall. Finally, while all effort was made to standardize care, individual

circumstances with each animal could have affected which medications they received, their

doses, and the timing of administration.

V. <u>CONCLUSIONS</u>

Our results suggest that asynchronous pulsatile modulation is an effective means to accomplish phasic ventricular volume unloading and greater physiologic aortic pulsatility while minimizing the risk of additional blood trauma. This study showed that it is feasible to asynchronously modulate the rotor speed of CF-VADs for long-term support to maintain near-physiologic pulsatility and reduce stroke volume with minimal hemolysis and increased power usage. The potential clinical impact of these findings is that chronic asynchronous modulation may be able to provide favorable conditions which could potentially reduce adverse event rates associated with CF-VAD use. Further studies using heart failure animals as the experimental platform may lead to a greater understanding of the volume unloading and aortic pulsatility effects of asynchronous pulsatile modulation.

REFERENCES CITED

Adamson, R. M., Dembitsky, W. P., Baradarian, S., Chammas, J., May-Newman, K., Chillcott, S., … Jaski, B. (2011). Aortic valve closure associated with HeartMate left ventricular device support: Technical considerations and long-term results. *The Journal of Heart and Lung Transplantation*, *30*(5), 576–582. https://doi.org/10.1016/j.healun.2010.11.007

Al-Gobari, M., Khatib, C. El, Pillon, F., & Gueyffier, F. (2013). Beta-blockers for the prevention of sudden cardiac death in heart failure patients: a meta-analysis of randomized controlled trials. *BMC Cardiovascular Disorders*, *13*(1), 52. https://doi.org/10.1186/1471-2261-13-52

Alraies, M. C., & Eckman, P. (2014). Adult heart transplant: indications and outcomes. *J Thorac Dis*, *6*(8), 1120–1128. https://doi.org/10.3978/j.issn.2072-1439.2014.06.44

Andrew, J., & Macdonald, P. (2015). Latest Developments in Heart Transplantation: A Review. *Clinical Therapeutics*, *37*(10), 2234–2241. https://doi.org/10.1016/j.clinthera.2015.08.019

Apostolakis, E., & Akinosoglou, K. (2007). Reexamining the New York Heart Association Functional Classification of Heart Failure. *The American Journal of Cardiology*, *100*(5), 911–912. https://doi.org/10.1016/j.amjcard.2007.05.006

Arakawa, M., Nishimura, T., Takewa, Y., Umeki, A., Ando, M., Kishimoto, Y., … Tatsumi, E. (2016). Pulsatile support using a rotary left ventricular assist device with an electrocardiography-synchronized rotational speed control mode for tracking heart rate variability. *Journal of Artificial Organs*, *19*(2), 204–207. https://doi.org/10.1007/s10047-015-0875-4

Barić, D. (2014). Why pulsatility still matters: a review of current knowledge. *Croatian Medical Journal*, *55*(6), 609–620. https://doi.org/10.3325/cmj.2014.55.609

Bartoli, C. R., & Atluri, P. (2015). Do patients with a continuous-flow left ventricular assist device benefit from induced-pulsatility or are we just spinning our wheels? *The Journal of Thoracic and Cardiovascular Surgery*, *150*(4), 945–946. https://doi.org/10.1016/j.jtcvs.2015.07.042

Bartoli, C. R., Giridharan, G. A., Litwak, K. N., Sobieski, M., Prabhu, S. D., Slaughter,

M. S., & Koenig, S. C. (2010). Hemodynamic Responses to Continuous versus Pulsatile Mechanical Unloading of the Failing Left Ventricle. *ASAIO Journal*, *56*(5), 410–416. https://doi.org/10.1097/MAT.0b013e3181e7bf3c

Bearnson, G. B., Olsen, D. B., Khanwilkar, P. S., Long, J. W., Allaire, P. E., & Maslen, E. H. (1996). Pulsatile Operation of a Centrifugal Ventricular Assist Device With Magnetic Bearings. *ASAIO Journal*, *42*(5), M620–M624.

Bourque, K., Dague, C., Farrar, D., Harms, K., Tamez, D., Cohn, W., … Frazier, O. H. (2006). In Vivo Assessment of a Rotary Left Ventricular Assist Device-induced Artificial Pulse in the Proximal and Distal Aorta. *Artificial Organs*, *30*(8), 638–642. https://doi.org/10.1111/j.1525-1594.2006.00276.x

Bozkurt, S., van Tuijl, S., Schampaert, S., van de Vosse, F. N., & Rutten, M. C. M. (2014). Arterial pulsatility improvement in a feedback-controlled continuous flow left ventricular assist device: An ex-vivo experimental study. *Medical Engineering & Physics*, *36*(10), 1288–1295. https://doi.org/10.1016/j.medengphy.2014.07.005

Copeland, J. G., Smith, R. G., Arabia, F. A., Nolan, P. E., Sethi, G. K., Tsau, P. H., … Slepian, M. J. (2004). Cardiac Replacement with a Total Artificial Heart as a Bridge to Transplantation. *New England Journal of Medicine*, *351*(9), 859–867. https://doi.org/10.1056/NEJMoa040186

Cowger, J., Pagani, F. D., Haft, J. W., Romano, M. A., Aaronson, K. D., & Kolias, T. J. (2010). The Development of Aortic Insufficiency in Left Ventricular Assist Device-Supported Patients. *Circulation: Heart Failure*, *3*(6), 668–674. https://doi.org/10.1161/CIRCHEARTFAILURE.109.917765

Date, K., Nishimura, T., Takewa, Y., Kishimoto, S., Arakawa, M., Umeki, A., … Tatsumi, E. (2016). Shifting the pulsatility by increasing the change in rotational speed for a rotary LVAD using a native heart load control system. *Journal of Artificial Organs*, *19*(4), 315–321. https://doi.org/10.1007/s10047-016-0906-9

Dickstein, K., Cohen-Solal, A., Filippatos, G., McMurray, J. J. V., Ponikowski, P., Poole-Wilson, P. A., … Zannad, F. (2008). ESC Guidelines for the diagnosis and treatment of acute and chronic heart failure 2008‡. *European Journal of Heart Failure*, *10*(10), 933–989. https://doi.org/10.1016/j.ejheart.2008.08.005

Earley, A., Persson, R., Garlitski, A. C., Balk, E. M., & Uhlig, K. (2014). Effectiveness of Implantable Cardioverter Defibrillators for Primary Prevention of Sudden Cardiac Death in Subgroups. *Annals of Internal Medicine*, *160*(2), 111–121. https://doi.org/10.7326/M13-1787

Ensminger, S. M., Gerosa, G., Gummert, J. F., & Falk, V. (2016). Mechanical Circulatory Support. *Innovations: Technology and Techniques in Cardiothoracic and Vascular Surgery*, *11*(5), 305–314. https://doi.org/10.1097/IMI.0000000000000305

Ferrari, M., Kruzliak, P., & Spiliopoulos, K. (2015). An insight into short- and long-term mechanical circulatory support systems. *Clinical Research in Cardiology*, *104*(2), 95–111. https://doi.org/10.1007/s00392-014-0771-6

Gilbert, E. M., & Xu, W. D. (2017). Rationales and choices for the treatment of patients with NYHA class II heart failure. *Postgraduate Medicine*, *129*(6), 619–631. https://doi.org/10.1080/00325481.2017.1344082

Gilotra, N. A., & Stevens, G. R. (2014). Temporary Mechanical Circulatory Support: A Review of the Options, Indications, and Outcomes. *Clinical Medicine Insights: Cardiology*, *8*(s1), 75–85. https://doi.org/10.4137/CMC.S15718

Goldstein, A. H., Monreal, G., Kambara, A., Spiwak, A. J., Schlossberg, M. L., Abrishamchian, A. R., & Gerhardt, M. A. (2005). Partial Support with a Centrifugal Left Ventricular Assist Device Reduces Myocardial Oxygen Consumption in Chronic, Ischemic Heart Failure. *Journal of Cardiac Failure*, *11*(2), 142–151. https://doi.org/10.1016/j.cardfail.2004.07.005

Goldstein, D. J., John, R., Salerno, C., Silvestry, S., Moazami, N., Horstmanshof, D., … Jorde, U. (2013). Algorithm for the diagnosis and management of suspected pump thrombus. *The Journal of Heart and Lung Transplantation*, *32*(7), 667–670. https://doi.org/10.1016/j.healun.2013.05.002

Greenwood, J. C., & Herr, D. L. (2014). Mechanical Circulatory Support. *Emergency Medicine Clinics of North America*, *32*(4), 851–869. https://doi.org/10.1016/j.emc.2014.07.009

Hall, J. E., & Guyton, A. C. (2011). *Textbook of medical physiology* (12th ed). Philadelphia, PA: Elsevier Saunders.

Hatano, M., Kinugawa, K., Shiga, T., Kato, N., Endo, M., Hisagi, M., … Nagai, R. (2011). Less Frequent Opening of the Aortic Valve and a Continuous Flow Pump Are Risk Factors for Postoperative Onset of Aortic Insufficiency in Patients With a Left Ventricular Assist Device. *Circulation Journal*, *75*(5), 1147–1155. https://doi.org/10.1253/circj.CJ-10-1106

Heidenreich, P. A., Albert, N. M., Allen, L. A., Bluemke, D. A., Butler, J., Fonarow, G. C., … Trogdon, J. G. (2013). Forecasting the Impact of Heart Failure in the United States: A Policy Statement From the American Heart Association. *Circulation: Heart Failure*, *6*(3), 606–619. https://doi.org/10.1161/HHF.0b013e318291329a

Horobin, J. T., Simmonds, M. J., Nandakumar, D., Gregory, S. D., Tansley, G., Pauls, J. P., … Fraser, J. F. (2018). Speed Modulation of the HeartWare HVAD to Assess In Vitro Hemocompatibility of Pulsatile and Continuous Flow Regimes in a Rotary Blood Pump. *Artificial Organs*. https://doi.org/10.1111/aor.13142

Hullin, R. (2014). Heart transplantation: current practice and outlook to the future. *Swiss Medical Weekly*, *144*(w13977). https://doi.org/10.4414/smw.2014.13977

Hunt, S. A., Abraham, W. T., Chin, M. H., Feldman, A. M., Francis, G. S., Ganiats, T. G., … Yancy, C. W. (2009). 2009 Focused Update Incorporated Into the ACC/AHA 2005 Guidelines for the Diagnosis and Management of Heart Failure in Adults: A Report of the American College of Cardiology Foundation/American Heart Association Task Force on Practice Guidelines: Develope. *Circulation*, *119*(14), e391–e479. https://doi.org/10.1161/CIRCULATIONAHA.109.192065

Ising, M., Sobieski, M. A., Slaughter, M. S., Koenig, S. C., & Giridharan, G. A. (2015). Feasibility of Pump Speed Modulation for Restoring Vascular Pulsatility with Rotary Blood Pumps. *ASAIO Journal*, *61*(5), 526–532. https://doi.org/10.1097/MAT.0000000000000262

Ising, M., Warren, S., Sobieski, M. A., Slaughter, M. S., Koenig, S. C., & Giridharan, G. A. (2011). Flow Modulation Algorithms for Continuous Flow Left Ventricular Assist Devices to Increase Vascular Pulsatility: A Computer Simulation Study. *Cardiovascular Engineering and Technology*, *2*(2), 90–100. https://doi.org/10.1007/s13239-011-0042-x

Kato, T. S., Chokshi, A., Singh, P., Khawaja, T., Cheema, F., Akashi, H., … Schulze, P. C. (2011). Effects of Continuous-Flow Versus Pulsatile-Flow Left Ventricular Assist Devices on Myocardial Unloading and Remodeling. *Circulation: Heart Failure*, *4*(5), 546–553. https://doi.org/10.1161/CIRCHEARTFAILURE.111.962142

Kemp, C. D., & Conte, J. V. (2012). The pathophysiology of heart failure. *Cardiovascular Pathology*, *21*(5), 365–371. https://doi.org/10.1016/j.carpath.2011.11.007

Kirklin, J. K., Pagani, F. D., Kormos, R. L., Stevenson, L. W., Blume, E. D., Myers, S. L., … Naftel, D. C. (2017). Eighth annual INTERMACS report: Special focus on framing the impact of adverse events. *The Journal of Heart and Lung Transplantation*, *36*(10), 1080–1086. https://doi.org/10.1016/j.healun.2017.07.005

Klabunde, R. E. (2012). *Cardiovascular physiology concepts* (2nd ed). Philadelphia, PA: Lippincott Williams & Wilkins/Wolters Kluwer.

Krum, H., & Abraham, W. T. (2009). Heart failure. *The Lancet*, *373*(9667), 941–955. https://doi.org/10.1016/S0140-6736(09)60236-1

Krum, H., & Teerlink, J. R. (2011). Medical therapy for chronic heart failure. *The Lancet*, *378*(9792), 713–721. https://doi.org/10.1016/S0140-6736(11)61038-6

Lampert, B. C., & Teuteberg, J. J. (2015). Right ventricular failure after left ventricular assist devices. *The Journal of Heart and Lung Transplantation*, *34*(9), 1123–1130. https://doi.org/10.1016/j.healun.2015.06.015

LaRose, J. A., Tamez, D., Ashenuga, M., & Reyes, C. (2010). Design Concepts and Principle of Operation of the HeartWare Ventricular Assist System. *ASAIO Journal*, *56*(4), 1. https://doi.org/10.1097/MAT.0b013e3181dfbab5

Lund, L. H., Khush, K. K., Cherikh, W. S., Goldfarb, S., Kucheryavaya, A. Y., Levvey, B. J., … Stehlik, J. (2017). The Registry of the International Society for Heart and Lung Transplantation: Thirty-fourth Adult Heart Transplantation Report—2017; Focus Theme: Allograft ischemic time. *The Journal of Heart and Lung Transplantation*, *36*(10), 1037–1046. https://doi.org/10.1016/j.healun.2017.07.019

May-Newman, K., Enriquez-Almaguer, L., Posuwattanakul, P., & Dembitsky, W. (2010). Biomechanics of the Aortic Valve in the Continuous Flow VAD-Assisted Heart. *ASAIO Journal*, *56*(4), 301–308. https://doi.org/10.1097/MAT.0b013e3181e321da

Maybaum, S., Epstein, S., Beniaminovitz, A., Di Tullio, M., Oz, M., Bergmann, S. R., & Mancini, D. (2002). Partial loading of the left ventricle during mechanical assist device support is associated with improved myocardial function, blood flow and metabolism and increased exercise capacity. *The Journal of Heart and Lung Transplantation*, *21*(4), 446–454. https://doi.org/10.1016/S1053-2498(01)00392-8

Mazurek, J. A., & Jessup, M. (2015). Understanding Heart Failure. *Cardiac Electrophysiology Clinics*, *7*(4), 557–575. https://doi.org/10.1016/j.ccep.2015.08.001

McMurray, J. J. V. (2010). Systolic Heart Failure. *New England Journal of Medicine*, *362*(3), 228–238. https://doi.org/10.1056/NEJMcp0909392

Metra, M., & Teerlink, J. R. (2017). Heart failure. *The Lancet*, *390*(10106), 1981–1995. https://doi.org/10.1016/S0140-6736(17)31071-1

Moazami, N., Dembitsky, W. P., Adamson, R., Steffen, R. J., Soltesz, E. G., Starling, R. C., & Fukamachi, K. (2015). Does pulsatility matter in the era of continuous-flow blood pumps? *The Journal of Heart and Lung Transplantation*, *34*(8), 999–1004. https://doi.org/10.1016/j.healun.2014.09.012

Monreal, G., Sherwood, L. C., Sobieski, M. A., Giridharan, G. A., Slaughter, M. S., & Koenig, S. C. (2014). Large animal models for left ventricular assist device research and development. *ASAIO Journal (American Society for Artificial Internal Organs : 1992)*, *60*(1), 2–8. https://doi.org/10.1097/MAT.0000000000000005

Morley, D., Litwak, K., Ferber, P., Spence, P., Dowling, R., Meyns, B., … Burkhoff, D. (2007). Hemodynamic effects of partial ventricular support in chronic heart failure: Results of simulation validated with in vivo data. *The Journal of Thoracic and Cardiovascular Surgery*, *133*(1), 21–28.e4. https://doi.org/10.1016/j.jtcvs.2006.07.037

National Research Council (US) Committee for the Update of the Guide for the Care and Use of Laboratory Animals. (2011). *Guide for the Care and Use of Laboratory Animals*. *Guide for the Care and Use of Laboratory Animals* (8th ed). Washington, D.C.: National Academies Press. https://doi.org/10.17226/12910

Pearse, S. G., & Cowie, M. R. (2014). Heart failure: Classification and pathophysiology. *Medicine (United Kingdom)*, *42*(10), 556–561. https://doi.org/10.1016/j.mpmed.2014.07.012

Pirbodaghi, T., Asgari, S., Cotter, C., & Bourque, K. (2014). Physiologic and hematologic concerns of rotary blood pumps: what needs to be improved? *Heart Failure Reviews*, *19*(2), 259–266. https://doi.org/10.1007/s10741-013-9389-4

Pirbodaghi, T., Axiak, S., Weber, A., Gempp, T., & Vandenberghe, S. (2012). Pulsatile control of rotary blood pumps: Does the modulation waveform matter? *The Journal of Thoracic and Cardiovascular Surgery*, *144*(4), 970–977. https://doi.org/10.1016/j.jtcvs.2012.02.015

Pirbodaghi, T., Cotter, C., & Bourque, K. (2014). Power Consumption of Rotary Blood

Pumps: Pulsatile Versus Constant-Speed Mode. *Artificial Organs*, *38*(12), 1024–1028. https://doi.org/10.1111/aor.12323

Potapov, E. V., Stepanenko, A., Krabatsch, T., & Hetzer, R. (2011). Managing long-term complications of left ventricular assist device therapy. *Current Opinion in Cardiology*, *26*(3), 237–244. https://doi.org/10.1097/HCO.0b013e328345af80

Potapov, E. V, Dranishnikov, N., Morawietz, L., Stepanenko, A., Rezai, S., Blechschmidt, C., … Krabatsch, T. (2012). Arterial wall histology in chronic pulsatile-flow and continuous-flow device circulatory support. *The Journal of Heart and Lung Transplantation*, *31*(11), 1171–1176. https://doi.org/10.1016/j.healun.2012.08.013

Prior, F., Gourlay, T., & Taylor, K. (1995). Pulse reverse osmosis: a new theory in the maintenance of fluid balance. *Perfusion*, *10*(3), 159–170. https://doi.org/10.1177/026765919501000307

Radovancevic, B., Vrtovec, B., De Kort, E., Radovancevic, R., Gregoric, I. D., & Frazier, O. H. (2007). End-organ Function in Patients on Long-term Circulatory Support With Continuous-or Pulsatile-flow Assist Devices. *J Heart Lung Transplant*, *26*, 815–818. Retrieved from https://www.jhltonline.org/article/S1053-2498(07)00404-4/pdf

Sarkar, K., & Kini, A. S. (2010). Percutaneous Left Ventricular Support Devices. *Cardiology Clinics*, *28*(1), 169–184. https://doi.org/10.1016/j.ccl.2009.09.007

Schroeder, M. J., Perreault, B., Ewert, D. L., & Koenig, S. C. (2004). HEART: an automated beat-to-beat cardiovascular analysis package using Matlab®. *Computers in Biology and Medicine*, *34*(5), 371–388. https://doi.org/10.1016/S0010-4825(03)00087-8

Shi, Y., Lawford, P. V, & Hose, D. R. (2010). Numerical Modeling of Hemodynamics with Pulsatile Impeller Pump Support. *Annals of Biomedical Engineering*, *38*(8), 2621–2634. https://doi.org/10.1007/s10439-010-0001-y

Slaughter, M. S., Giridharan, G. A., Tamez, D., LaRose, J., Sobieski, M. A., Sherwood, L., & Koenig, S. C. (2011). Transapical miniaturized ventricular assist device: Design and initial testing. *The Journal of Thoracic and Cardiovascular Surgery*, *142*(3), 668–674. https://doi.org/10.1016/j.jtcvs.2011.01.011

Soucy, K. G., Giridharan, G. A., Choi, Y., Sobieski, M. A., Monreal, G., Cheng, A., … Koenig, S. C. (2015). Rotary pump speed modulation for generating pulsatile flow and phasic left ventricular volume unloading in a bovine model of chronic ischemic heart failure. *The Journal of Heart and Lung Transplantation*, *34*(1), 122–131. https://doi.org/10.1016/j.healun.2014.09.017

Takeda, J. (1960). Experimental study of peripheral circulation during extracorporeal circulation with a special reference to a comparison of pulsatile flow with non-pulsatile flow. *Arch Jap Chir*, *29*(6), 1407–1430. Retrieved from https://repository.kulib.kyoto-u.ac.jp/dspace/bitstream/2433/207188/1/ngh029006_1407.pdf

Tamez, D., LaRose, J. A., Shambaugh, C., Chorpenning, K., Soucy, K. G., Sobieski, M. A., … Slaughter, M. S. (2014). Early Feasibility Testing and Engineering Development of the Transapical Approach for the HeartWare MVAD Ventricular Assist System. *ASAIO Journal*, *60*(2), 170–177. https://doi.org/10.1097/MAT.0000000000000038

Tanai, E., & Frantz, S. (2015). Pathophysiology of Heart Failure. In *Comprehensive Physiology* (Vol. 6, pp. 187–214). Hoboken, NJ, USA: John Wiley & Sons, Inc. https://doi.org/10.1002/cphy.c140055

Toda, K., & Sawa, Y. (2015). Clinical management for complications related to implantable LVAD use. *General Thoracic and Cardiovascular Surgery*, *63*(1), 1–7. https://doi.org/10.1007/s11748-014-0480-0

Travis, A. R., Giridharan, G. A., Pantalos, G. M., Dowling, R. D., Prabhu, S. D., Slaughter, M. S., … Koenig, S. C. (2007). Vascular pulsatility in patients with a pulsatile- or continuous-flow ventricular assist device. *The Journal of Thoracic and Cardiovascular Surgery*, *133*(2), 517–524. https://doi.org/10.1016/j.jtcvs.2006.09.057

Umeki, A., Nishimura, T., Ando, M., Takewa, Y., Yamazaki, K., Kyo, S., … Tatsumi, E. (2012). Alteration of LV end-diastolic volume by controlling the power of the continuous-flow LVAD, so it is synchronized with cardiac beat: development of a native heart load control system (NHLCS). *Journal of Artificial Organs*, *15*(2), 128–133. https://doi.org/10.1007/s10047-011-0615-3

Umeki, A., Nishimura, T., Ando, M., Takewa, Y., Yamazaki, K., Kyo, S., … Tatsumi, E. (2013). Change of Coronary Flow by Continuous-Flow Left Ventricular Assist Device With Cardiac Beat Synchronizing System (Native Heart Load Control System) in Acute Ischemic Heart Failure Model. *Circulation Journal*, *77*(4), 995–1000. https://doi.org/10.1253/circj.CJ-12-0676

Umeki, A., Nishimura, T., Takewa, Y., Ando, M., Arakawa, M., Kishimoto, Y., … Tatsumi, E. (2013). Change in myocardial oxygen consumption employing continuous-flow LVAD with cardiac beat synchronizing system, in acute ischemic heart failure models. *Journal of Artificial Organs*, *16*(2), 119–128. https://doi.org/10.1007/s10047-012-0682-0

Underwood, W. J., Blauwiekel, R., Delano, M. L., Gillesby, R., Mischler, S. A., & Schoell, A. (2015). Biology and Diseases of Ruminants (Sheep, Goats, and Cattle). In *Laboratory Animal Medicine* (pp. 623–694). Elsevier. https://doi.org/10.1016/B978-0-12-409527-4.00015-8

Yancy, C. W., Jessup, M., Bozkurt, B., Butler, J., Casey, D. E., Drazner, M. H., … Wilkoff, B. L. (2013). 2013 ACCF/AHA Guideline for the Management of Heart Failure. *Journal of the American College of Cardiology*, *62*(16), e147–e239. https://doi.org/10.1016/j.jacc.2013.05.019

Yang, F., Kormos, R. L., & Antaki, J. F. (2015). High-speed visualization of disturbed pathlines in axial flow ventricular assist device under pulsatile conditions. *The*

Journal of Thoracic and Cardiovascular Surgery, *150*(4), 938–944. https://doi.org/10.1016/j.jtcvs.2015.06.049

Zannad, F., McMurray, J. J. V., Krum, H., van Veldhuisen, D. J., Swedberg, K., Shi, H., … Pitt, B. (2011). Eplerenone in Patients with Systolic Heart Failure and Mild Symptoms. *New England Journal of Medicine*, *364*(1), 11–21. https://doi.org/10.1056/NEJMoa1009492

VITA

Connor Joseph Smith
Graduate Student
Department of Bioengineering
University of Louisville
Louisville, KY
connor.smith@louisville.edu

Education

Future (Fall 2018)   University of Louisville
                         School of Medicine
                         Class of 2022

2017 – Present   University of Louisville
                         JB Speed School of Engineering
                         Master of Engineering
                         Department: Bioengineering

2013 – 2017   University of Louisville
                         JB Speed School of Engineering
                         Bachelor of Science
                         Department: Bioengineering
                         With Honors

Academic and Professional Experience

May 2017 – Present   M.Eng. Student Research Assistant
                         Advanced Heart Failure Research Group
                         Cardiovascular Innovations Institute, UofL

Aug. 2015 – May 2017	Bioengineering Research Co-op Advanced Heart Failure Research Group Cardiovascular Innovations Institute, UofL
Dec. 2015 – Dec 2016	President Sigma Pi Fraternity Intl., Iota-Omicron Chapter University of Louisville
Aug 2014 – Dec 2015	Vice President Sigma Pi Fraternity Intl., Iota-Omicron Chapter University of Louisville

Awards and Recognition

2017	Rolando Chip Cheng, Jr. Memorial Award University of Louisville Bioengineering Department
2015	Tau Beta Pi Engineering Honor Society Initiation University of Louisville Chapter
2013	Trustees Scholarship Award – Full Tuition University of Louisville

Organizational Memberships

2014 – Present	Sigma Pi Fraternity International
2013 – Present	Biomedical Engineering Honor Society
2015 – 2017	Tau Beta Pi Engineering Honor Society

Abstracts

1. **Smith CJ**, Sobieski MA, Monreal G, Adams T, Soucy KG, Gallo M, Whited WM, Kohl A, Slaughter MS, Koenig SC. Rotary pump speed modulation to produce pulsatile flow and phasic ventricular volume unloading. Accepted as a poster presentation, BMES Annual Meeting 2018.

2. Tapolsky NR, Tompkins LH, **Smith CJ**, Ebersold NR, Sobieski MA, Monreal G, Polverelli L, Monticone P, Botterbusch C, Slaughter MS, Koenig SC. In vitro performance of a novel membrane-oscillating left ventricular assist device. Accepted as an oral presentation, ASAIO Conference 2017.

Presentations

1. **Smith CJ**. Predicting myocardial growth during heart failure. Student, BE600 – Modeling of Biological Phenomena. J.B. Speed School of Engineering, University of Louisville, Louisville KY. July 11th, 2017.

2. **Smith CJ**. A review of heparin-induced thrombocytopenia and its effects on cardiac patients. Student, BE611 – Cardiovascular Dynamics. J.B. Speed School of Engineering, University of Louisville, Louisville KY. July 7th, 2017.

3. **Smith CJ**. Cardiostimulatory drugs and their effects on underlying cardiovascular dynamics. Student, BE611 – Cardiovascular Dynamics. J.B. Speed School of Engineering, University of Louisville, Louisville KY. June 26th, 2017.

4. **Smith CJ**, NeCamp S, Pack L, Cory D. Supplies Over Seas Inventory Application System Development. Student, BE497 – Bioengineering Design Project. J.B. Speed School of Engineering, University of Louisville, Louisville KY. December 12th, 2016.

5. **Smith CJ**, Hodge D, Pack L. High efficiency cell-recycle continuous sodium gluconate production by *Aspergillus niger* using on-line physiological parameters association analysis to regulate feed rate rationally: A Review. Student, BE430 – Biosystems Controls. J.B. Speed School of Engineering, University of Louisville, Louisville KY. December 5th, 2016.

6. **Smith CJ**, Barrow B. Development of a partially automated cardiopulmonary bypass. Student, BE480 – Biomedical Device Design. J.B. Speed School of Engineering, University of Louisville, Louisville KY. April 15th, 2016.

7. **Smith CJ**, Barrow B. A review of extra-corporeal membrane oxygenation. Student, BE480 – Biomedical Device Design. J.B. Speed School of Engineering, University of Louisville, Louisville KY. February 15th, 2016.

8. **Smith CJ**, Simms L, Pack L. PEGylated fluorescent Potato Virus X as an optical imaging probe to increase bioavailability. Student, BE450 – Biomaterials and Biocompatibility. J.B. Speed School of Engineering, University of Louisville, Louisville KY. July 14th, 2015.